Identification of critical effect factors for prediction of spatial and intra-annual variability of shallow groundwater nitrate in agricultural areas

Chunying Wang, Xinliang Wang, Gengchen Zhang, Feifei Zhang, Junfeng Li, Shuai Chen, Sabine Sauvage, José-Miguel Sánchez-Pérez, Yuping Han, Junguo Liu

Prediction of spatial and intra-annual variability of shallow groundwater nitrate in agricultural areas

Chunying Wang[a*], Xinliang Wang[a], Gengchen Zhang[a], Feifei Zhang[a], Junfeng Li[b], Shuai Chen[a], Sabine Sauvage[c], José-Miguel Sánchez-Pérez[c], Yuping Han[a], Junguo Liu[a,d]

[a] *School of Water Resources, North China University of Water Resources and Electric Power, Zhengzhou 450045, PR China;*

[b] *College of Water Conservancy and Architecture Engineering, Shihezi University, Shihezi 832000, PR China;*

[c] *Laboratory of Functional Ecology and Environment, University of Toulouse, CNRS, UPS, Toulouse INP, ENSAT campus, F-31326 Toulouse, France*

[d] *School of Environmental Science and Engineering, Southern University of Science and Technology, Shenzhen 518055, PR China;*

A B S T R A C T

Shallow groundwater nitrate nitrogen (NO_3^--N) concentrations in agricultural areas usually show high spatial and intra-annual variability. It is hard to predict such concentrations due to the complexity of influencing factors (e.g., different forms of N in soil, vadose zone characteristics, and groundwater environmental conditions). Here, a large number of groundwater and soil samples were collected monthly over two years at 14 sites to analyze the soil and groundwater physiochemical properties and the stable isotopes of $\delta^{15}N$ and $\delta^{18}O$ of groundwater NO_3^--N in agricultural areas. Based on field observations, a random forest (RF) model was used to predict the groundwater NO_3^--N concentrations and reveal the importance of effect factors. The results show that there are large spatiotemporal variations in NO_3^--N, $\delta^{15}N$-NO_3^-, and $\delta^{18}O$-NO_3^- in groundwater. NO_3^--N is the major dominant specie

of inorganic N in groundwater, and the groundwater NO_3^--N concentration in 24% of the samples failed to meet the drinking water standard of the WHO (10 mg L^{-1}). The RF model satisfactorily predicted groundwater NO_3^--N concentrations with R^2 of 0.92–0.93, RMSE of 3.87–4.94, and MAE of 2.10–2.89. Groundwater nitrite and ammonium are the most important factors related to NO_3^--N removal and production in groundwater. Denitrification and nitrification were further identified by the relationships among $\delta^{15}N\text{-}NO_3^-$, $\delta^{18}O\text{-}NO_3^-$, and NO_3^--N, and by the ranges of $\delta^{15}N\text{-}NO_3^-$, $\delta^{18}O\text{-}NO_3^-$, temperature, pH, DO, and ORP in groundwater. Soil-soluble organic nitrogen (S-SON) and the depth of groundwater table were identified as vital factors related to N sourcing and leaching. Overall, as a first approach to adopting a RF model for high spatiotemporal-resolution prediction of groundwater NO_3^--N variations, the findings of this study enable a better understanding of groundwater N pollution in agricultural areas. Optimizing management of irrigation and N inputs is anticipated to reduce S-SON accumulation and mitigate the threat to groundwater quality in agricultural areas.

Keywords: Groundwater nitrate; Effect factor; Nitrogen transformation; Random forest; Nitrogen and oxygen isotopes

1. Introduction

Groundwater is currently facing the severe challenges of depletion and deteriorating quality due to natural and anthropogenic factors around the world (Liu et al., 2016; Famiglietti and Ferguson, 2021). Among the many groundwater problems, nitrogen (N) pollution has become a global issue due to the use of N fertilizers and manures and elevated atmospheric deposition (Vystavna et al., 2017). Groundwater N pollution reduces N use efficiency and threatens the safety of the water supply in China (Gan et al., 2022; Gao et al., 2022). The nitrate nitrogen (NO_3^--N) contamination of groundwater is a severe problem threatening the environment and human health, especially in intensively irrigated agricultural areas. Accurately predicting the variations of shallow groundwater NO_3^--N concentrations at high spatiotemporal resolution is very difficult due to the complex effect factors and processes (Hinkle and Tesoriero, 2014; Biddau et al., 2019; He et al., 2022). Therefore, exploration of the spatiotemporal patterns and any associated effect factors and processes is urgently needed to prevent widespread water-quality issues around the world.

Climate variables, soil texture, land use, and human activities are commonly investigated and recognized as the main factors affecting the inter-annual variations of groundwater NO_3^--N pollution on the large or macroscopic scale (Pennino et al., 2020; El Amri et al., 2022; He et al., 2022). Nonetheless, comprehensive identification of the effect factors and evaluation of their impact on dynamics of groundwater NO_3^--N has seldomly been done at a high spatial and monthly temporal resolution, especially in irrigated agricultural areas. Climate variables and agricultural management activities, such as

precipitation, irrigation, and fertilizer input, cause the high level of variability in the different forms of N content in soil and subsequent leaching to groundwater. Vadose zone thickness (i.e., the depth of the groundwater table) contributes significantly to the variations of groundwater NO_3^--N concentrations by affecting the amounts of different forms of N leaching and groundwater environmental conditions (Li et al., 2021; Weitzman et al., 2022). Meanwhile, groundwater environmental parameters influence the different forms of N content by impacting transformation processes. Environmental factors related to N transformation in groundwater include temperature, dissolved oxygen (DO), oxidation-reduction potential (ORP), and dissolved organic carbon (DOC). The difficulty in understanding groundwater NO_3^--N variations stems from the ability to determine the most critical explanatory variables among the many factors. This question is challenging when using common traditional methods, such as correlation analysis, attribution analysis, cluster analysis, principal component analysis, and numerical and distributed hydrological models.

Overall, groundwater NO_3^--N concentrations are controlled by diverse factors that are linked through the complex interaction of multiple processes. These processes involve inorganic and organic N transformation and transport in soil and groundwater (Zhang et al., 2019). Surface soil N leaching to groundwater and the groundwater environment are both affected by characteristics of the vadose zone. The leaching of different forms of N content from the surface soil, as the source of N in groundwater, indirectly affects groundwater NO_3^--N dynamics through N transformation in groundwater. The N transformation in groundwater is affected by the groundwater environment, and it increases the importance

and difficulty of identifying the roles of N transformation in groundwater. In terms of the N in groundwater, the widely reported mineralization, nitrification, and denitrification processes in groundwater can modify different forms of N species balance (Liu et al., 2022; Shen et al., 2023). For instance, the mineralization and nitrification processes in groundwater can produce NO_3^--N, while denitrification can reduce NO_3^--N. These processes in groundwater play a key influence in the spatiotemporal variations of NO_3^--N dynamics in addition to N leaching in soil. Therefore, identifying the main N transformation processes in groundwater and evaluating their importance will further elucidate the mechanisms of groundwater NO_3^--N pollution in agricultural areas.

The complex factors and processes influencing groundwater NO_3^--N concentrations lead to great difficulty in making predictions at high spatial and temporal resolution. For instance, physically based numerical and distributed hydrological models (e.g., HYDRUS, AgriFlux, and SWAT [Soil & Water Assessment Tool]) need to be coupled with groundwater flow models, such as MODFLOW-MT3D and the model of Lasserre et al. (1999) linked to a GIS (geographic information system), to predict groundwater NO_3^--N dynamics (Wang et al., 2016; El Amri et al., 2022). The performance of these models basically depends on an adequate understanding of hydrological behaviors and biogeochemical processes and the availability of detailed data on the properties of the vadose zone and groundwater system. These data are usually difficult to measure and collect, resulting in unsatisfactory model performance (Coppola et al., 2005). Machine learning methods, for example, artificial neural networks, multiple logistic regressions,

generalized additive models, generalized linear models, support vector regressions, and random forest models, have been widely used to predict the N status in agricultural and natural waste waters (Chlingaryan et al., 2018; Bagherzadeh et al., 2021; He et al., 2022). They were gradually accepted by researchers due to their advantages, such as their high generalization ability and low cost, but most of them have the problem of overfitting (Castrillo and García, 2020). Among these machine learning methods, the random forest model has the advantages of strong resistance to overfitting, no feature selection, and automatic data filling. It has been proven to accurately predict inter-annual groundwater NO_3^--N concentrations on a large scale (Band et al., 2020; He et al., 2022). However, the random forest model has not yet been applied to predict intra-annual variations of shallow groundwater NO_3^--N in irrigated agricultural areas.

The North China Plain (NCP) is the main crop production area in China, and groundwater resources in the NCP are generally dealing with the issue of N pollution. This study was conducted in a semiarid heavily irrigated agricultural area located in the NCP, that is characterized by a shallow groundwater table depth and, thus, vulnerable to groundwater pollution. Monthly meteorological data were obtained from the Xinxiang weather station, which is located near the study site. Two years' worth of monthly soil physiochemical data and groundwater quality parameters were measured in the field and laboratory. The objectives of this study were to: (1) reveal the spatial and intra-annual variations of inorganic N species and isotopic signature of NO_3^--N in groundwater, (2) construct a random forest model to predict spatiotemporal variations of groundwater

NO_3^--N using a simplified approach to the model, and (3) identify the main effect factors and processes, and evaluate their relationships with groundwater NO_3^--N based on the constructed random forest model and isotope approaches. The ability to prediction the levels of groundwater NO_3^--N pollution and uncover the mechanism that underlies its high spatial and temporal variability is important for future management of agricultural N input and water-quality protection in all developing and developed countries.

2. Materials and Methods

2.1. Site description

This study was conducted in an irrigated agricultural area (35°00′– 35°30′ N, 113°31′–114°25′ E) located in the piedmont region of Taihang mountain, NCP, near the lower reaches of the Yellow River (Fig. 1). The study site covers about 1,500 km^2 and belongs to the temperate continental monsoon climate. Weather data from Xinxiang station, located near our study site, were obtained from the China Meteorological Data Service Center (http://data.cma.cn/). From 2010 to 2019, the average annual temperature was 15.6°C, with a maximum temperature of 40°C and a minimum temperature of -13.1°C.The average annual potential evaporation was 1,025 mm yr^{-1}, and the average annual rainfall was about 500 mm yr^{-1}. The rainfall mainly occurred from June to September. According to the aquifer data collected by field surveys, the average annual groundwater table depth ranged from 1.9 to 18 m, and the groundwater level ranged from 54.1 to 82.4 m (Fig. 1a–b). The particle size of the soil was analyzed using a Malvern laser particle size analyzer as reported in our previous study (Wang et al., 2021). According to the international soil texture classification standard, the soil in the study area was classified into silt (8.3%), silty loam (61.1%), and sandy loam (30.6%) (Fig. 1c). The main crops were winter wheat and summer maize (44%), winter wheat and summer peanut (27%), and winter wheat and summer rice (11%) at the study site

(Fig. 1d). Other land uses, including rural residential areas, urban areas, and water body areas, constitute the remaining 18% of the study site (Fig. 1d). Irrigation and fertilization play important roles in ensuring stable crop production and the N applied on the agricultural land surface was mainly derived from chemical fertilizers, manure, and crop residues. The crop residues of winter wheat and summer corn/summer peanuts were all returned to the fields. The large amount and temporal variability in N input causes the groundwater N content to show high spatiotemporal variations and increase continuously, which poses a serious burden on groundwater N pollution and its management.

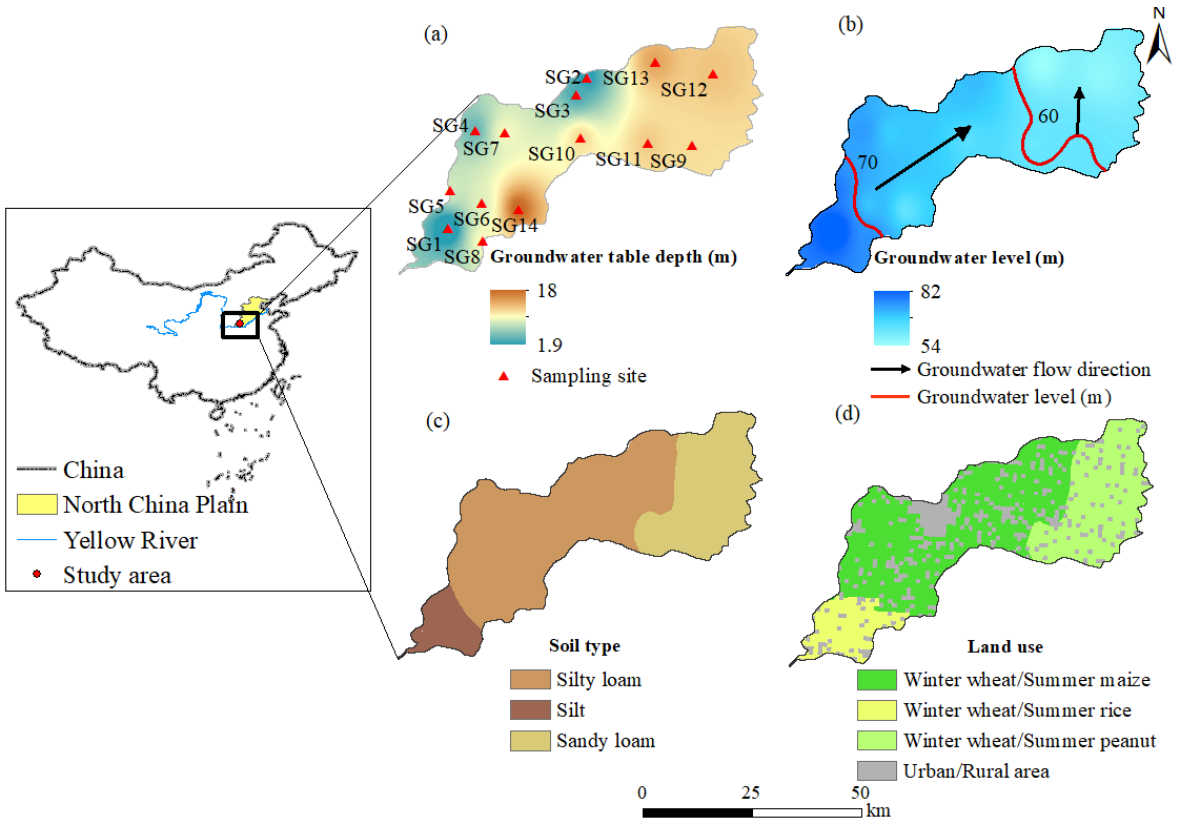

Fig. 1. Location of the study area in the North China Plain and the sampling sites, and maps of (a) the depth of the groundwater table, (b) the groundwater level, (c) the soil type and (d) land use. The land use map was obtained from the Geospatial Data Cloud (http://www.gscloud.cn/search)

2.2. Field monitoring, sampling and chemical analysis

Fourteen representative sampling sites were selected according to the geographical location, land use, soil types, and the groundwater table depth to conduct field monitoring and collect surface soil and groundwater samples (Fig. 1a and Table 1). The field

monitoring and sample collection were conducted monthly from May 2017 to April 2019 at the 14 observation sites (Fig. 1a). The field monitoring involved the use of a multiparameter water quality probe (HORIBA, Ltd., Japan) to determine the basic physicochemical parameters of groundwater, including water temperature (GW-Temp), pH (GW-pH), total dissolved solids concentration (GW-TDS), oxidation-reduction potential (GW-ORP), and dissolved oxygen (GW-DO). At the same time, the depth of the groundwater table (GW-Dep) was measured and groundwater water samples were collected using a bailer tube. The data on irrigation were collected through a survey of the local farmers.

Table 1. Soil texture, crops, depth of groundwater table, and groundwater level at sampling sites

Sampling site	Soil texture	Crop rotation	Groundwater table depth (m)	Groundwater level (m)
SG1	Silt	Winter wheat-summer rice	2	82.4
SG2	Silty loam	Winter wheat-summer corn	3.9	65.5
SG3	Silty loam	Winter wheat-summer corn	4.9	65.9
SG4	Silty loam	Winter wheat-summer corn	6	69.3
SG5	Silty loam	Winter wheat-summer corn	9.4	74.5
SG6	Silty loam	Winter wheat-summer corn	9.9	64.5
SG7	Silty loam	Winter wheat-summer corn	10.5	63.6
SG8	Silty loam	Winter wheat-summer corn	10.7	71.5
SG9	Sandy loam	Winter wheat-summer peanuts	12.2	60.1
SG10	Silty loam	Winter wheat-summer corn	12.3	60.8
SG11	Sandy loam	Winter wheat-summer peanuts	12.9	58.8
SG12	Sandy loam	Winter wheat-summer peanuts	13.3	55.2
SG13	Silty loam	Winter wheat-summer corn	14.8	54.1
SG14	Silty loam	Winter wheat-summer corn	18	60.1

Groundwater and soil samples were collected at a frequency of once a month during the two-year study period. The groundwater samples were collected from wells and filtered using a 0.45 μm filter. These groundwater samples were brought back to the laboratory, and 1 L of each sample was stored in a refrigerator at a temperature of 2°C until physiochemical analysis. At the same time, 100 ml groundwater samples were immediately frozen until

isotope analysis. Moreover, soil samples were collected from farmland within 500 m of the wells where the groundwater samples were collected. The soil samples were gathered at the soil surface with a depth of 0–10 cm in the farmland. All the soil samples were randomly collected from six sites and mixed thoroughly to obtain a representative soil sample (500 g) at each sampling site. Meanwhile, additional soil samples were collected in aluminum boxes that were sealed and brought back to the laboratory. The mixed soil samples were dried naturally, crushed through a 2 mm sieve, and stored in a cool and dry place until physiochemical analysis.

The soil samples stored in the aluminum boxes were further used to analyze the soil water content (SWC) through the oven-drying method. The parameters measured in the laboratory include groundwater dissolved organic carbon (GW-DOC), groundwater dissolved organic N (GW-DON), groundwater ammonium (GW-NH_4^+-N), groundwater nitrate (GW-NO_3^--N), groundwater nitrite (GW-NO_2^--N), soil organic carbon (SOC), soil-soluble organic N (S-SON), soil nitrate (S-NO_3^--N), soil nitrite (S-NO_2^--N), and soil ammonium (S-NH_4^+-N). All these chemical parameters of soil and groundwater were determined by the colorimetric method using a spectrophotometer (Thermo Fisher Scientific, Inc, USA) according to the procedures reported by Hood-Nowotny et al. (2010) and Wang et al. (2021).

Since August 2018, the influence of N leaching on groundwater has been weaker in the following eight-month dry period than in the wet period. Therefore, in this study the isotope analysis was performed on groundwater samples to identify nitrification and denitrification in groundwater from August 2018 to April 2019. The stable isotope (^{15}N and ^{18}O)

abundance of groundwater NO_3^--N was determined using the denitrifying bacteria method. A seed solution (of glycerol 500 μL + bacteria 500 μL) was shaken for 12–15 hrs, purged with N_2 for 3 hrs, and then added to the sample and placed in a shaking table at 100 rpm overnight, shaking and as determined by an IRMS-100 mass spectrometer. USG32, USG34, and USG35 were used as standard samples, and the results were corrected based on a two-point calibration method. The measured isotope values correspond to the international standard substances, expressed as follows:

$$\delta_{sample}(‰) = \frac{R_{sample} - R_{VSMOW}}{R_{VSMOW}} \times 1000 \quad [1]$$

where δ_{sample} is the isotope value of the corresponding sample, R_{sample} is the ratio of heavy and light isotopic abundance of elements in the sample, and R_{VSMOW} is the ratio of heavy and light isotopic abundance of Vienna Standard Mean Ocean Water (VSMOW).

2.3. Random forest model

A random forest model was used to predict the intra-annual variations of groundwater NO_3^--N at the study site. The random forest model is a machine learning algorithm based on the combination of the bagging integrated learning theory and the random subspace algorithm, and it overcomes the drawbacks of overfitting and instability (Breiman, 2001). The model constructs several regression trees (ntree) by setting nodes (mtry) on a random subset of the original training dataset, according to Amit and Geman (1997). The random forest model divides the data into training and test sets by setting a certain ratio (P), and the P ratio of 2:1 was chosen in this study. The random forest model was then calibrated using the training subset and validated using the test subset. A package of *randomForest* in Rstudio (version 4.2.2) was adopted to construct the random forest model.

The model accuracy was made to meet the research needs by adjusting the three parameters ntree, mtry, and P. Three error metrics, the root mean square error (RMSE), the coefficient of determination (R^2), and the mean absolute error (MAE), were selected to evaluate the random forest model's performance. The trained and validated random forest model was used to analyze the importance of groundwater NO_3^--N influencing factors. The importance of an effect factor is defined as the increase in the predicted mean squared error (MSE) after randomly permuting this factor (Breiman, 2001). It reflects the contribution of each effect factor to a groundwater nitrate concentration. The normalized increased MSE, that is, the relative importance, for each effect factor was between 0% and 100%. The partial dependence shows the marginal effect of each explanatory variable for the response after considering the average effects of the other variables. The partial dependence plots of the important effect factors were used to analyze the relationship between a single independent variable and the groundwater NO_3^--N subject to the influence of the other independent variables.

2.4. Data analysis

The spatial distribution of the measured data was interpolated using inverse distance weighting in ArcGIS to analyze the spatial distribution characteristics of different N species in groundwater from the study site. The Spearman coefficient (r), paired t-tests, and a one-way analysis of variance (ANOVA) were used to calculate the correlation coefficient and test the significance using SPSS software (version 25.0, IBM Corporation, Chicago, Illinois). Denitrification was identified based on NO_3^--N isotopes and their relationships, that is, the enrichment of $\delta^{15}N\text{-}NO_3^-$ and $\delta^{18}O\text{-}NO_3^-$ with a slope of 0.5–1.0 ($\Delta\delta^{18}O/\delta^{15}N$),

and a decrease of NO_3^--N concentrations. An increase of NO_3^--N concentrations and decrease of $\delta^{15}N\text{-}NO_3^-$ and $\delta^{18}O\text{-}NO_3^-$ were analyzed to identify nitrification.

3. Results and Discussion

3.1. Statistical analysis of groundwater nitrate concentration and its effect factors

Table 2 lists the variables analyzed in this study, that is, the precipitation, irrigation, soil sand content (SSC), SWC, SOC, S-SON, S-NO_3^--N, S-NH_4^+-N, S-NO_2^--N, GW-NO_3^--N, GW-NH_4^+-N, GW-NO_2^--N, GW-DON, GW-DOC, GW-Dep, GW-Temp, GW-TDS, GW-pH, GW-DO, and GW-ORP. The 19 predictor variables in Table 2 were considered as effect factors that could potentially influence groundwater GW-NO_3^--N. The maximum, minimum and mean values; standard deviation (SD); coefficient of variation (CV); and quartile of these variabiles are shown in Table 2. Different forms of N content from surface soil were considered instead of N input due to the complex sources and transformation processes of N input. The statistical characteristics of N input were not analyzed. As shown in Table 2, all the CV values, which can reflect the size of dispersion of the measured data, ranged from 0.08 to 2.06, and most of the factors had small CVs and low variability. However, the CV values of groundwater inorganic N were all greater than 1, indicating that spatial and temporal patterns of groundwater inorganic N concentrations were highly variable in the study area. The SD and CV of groundwater NO_3^--N concentrations were the largest compared with NH_4^+-N and NO_2^--N, indicating that the spatiotemporal variability of groundwater NO_3^--N concentrations was the highest among the three forms of inorganic N.

Table 2 Summary statistics of the variables analyzed in this study (May 2017-April 2019)

	Variables	Max	Min	Mean	SD	CV	Quartiles		
							25th	50th	75th
Predictor variables, i.e., the effect factors that could potentially influence GW-NO_3^--N	Precipitation (mm)	98.20	0.20	35.47	33.07	0.93	4.78	26.65	67.95
	Irrigation (mm)	300.0	0.00	96.10	93.25	0.97	0.00	105.00	200.00
	GW-Dep (m)	19.00	0.10	10.03	4.48	0.45	5.82	10.90	13.03
	SSC (%)	71.26	12.45	31.10	16.60	0.53	21.40	25.70	28.2
	SWC (mg mg^{-1})	0.42	0.01	0.16	0.09	0.54	0.09	0.16	0.22
	SOC (g kg^{-1})	37.19	0.75	16.80	6.83	0.41	11.57	16.19	21.91
	S-SON (mg kg^{-1})	805.50	34.55	333.62	146.32	0.44	209.80	335.06	440.33
	S-NO_3^--N (mg kg^{-1})	265.10	6.87	53.89	47.22	0.88	25.57	38.00	59.64
	S-NO_2^--N (mg kg^{-1})	11.40	0.01	2.74	1.80	0.66	1.68	2.28	3.15
	S-NH_4^+-N (mg kg^{-1})	62.80	6.41	18.99	7.12	0.38	14.89	18.49	22.25
	GW-pH	8.70	3.42	7.14	0.58	0.08	6.84	7.13	7.52
	GW-Temp (℃)	31.20	6.95	18.40	4.07	0.22	15.56	17.85	20.80
	GW-DO (mg L^{-1})	50.00	2.65	11.78	7.28	0.62	7.31	9.91	13.37
	GW-ORP (mV)	308.0	-136.0	137.24	120.67	0.88	46.25	172.50	235.00
	GW-DOC (mg L^{-1})	280.30	<LOD	42.84	43.27	1.01	13.35	25.83	64.60
	GW-TDS (g L^{-1})	3.17	0.22	1.15	0.65	0.56	0.73	0.95	1.30
	GW-DON (mg L^{-1})	808.38	<LOD	69.40	78.20	1.13	25.70	69.40	73.30
	GW-NO_2^--N (mg L^{-1})	0.52	<LOD	0.08	0.11	1.49	0.01	0.03	0.07
	GW-NH_4^+-N (mg L^{-1})	22.80	0.04	1.52	1.61	1.05	0.77	1.23	1.93
Response variable	GW-NO_3^--N (mg L^{-1})	132.20	0.09	8.31	14.77	1.78	1.60	3.60	9.24

Note: standard deviation (SD), coefficient of variation (CV), depth of groundwater table (GW-Dep), soil sand content (SSC), soil water content (SWC), soil organic carbon content (SOC), soil soluble organic N content (S-SON), soil nitrate content (S-NO_3^--N), soil nitrite content (S-NO_2^--N), soil ammonium content (S-NH_4^+-N), groundwater pH (GW-pH), groundwater temperature (GW-Temp), groundwater dissolved oxygen content (GW-DO), groundwater oxidation-reduction potential (GW-ORP), groundwater dissolved organic carbon concentration (GW-DOC), groundwater total dissolved solids (GW-TDS), groundwater dissolved organic N concentration (GW-DON), groundwater ammonium concentration (GW-NH_4^+-N), groundwater nitrite concentration

(GW-NO_2^--N), groundwater nitrate concentration (GW-NO_3^--N), Limit of detection (LOD).

3.2. Spatiotemporal variations of inorganic N species in groundwater

The temporal and spatial variations of groundwater inorganic N concentrations in the study area are shown in Figs. 2–3. There is a large difference in the temporal variations of groundwater inorganic N concentrations (Fig. 2a–c). The groundwater NO_3^--N concentrations ranged from 0.09 to 132.16 mg L^{-1}. The groundwater NO_3^--N concentrations were higher from May to August and usually decreased from September to April of the following year. In this study, the peaks of the groundwater NO_3^--N concentrations were caused by high level of NO_3^--N leaching after fertilization, irrigation, and heavy rain in the rainy season (May–August). This result is consistent with the previous findings of Biddau et al. (2019), who reported the high levels of NO_3^--N concentrations (up to 162 mg L^{-1}) in shallow groundwater also occur when NO_3^--N leaching is high, particularly during fertilization and irrigation periods. The groundwater NH_4^+-N concentrations ranged from 0.04 to 22.8 mg L^{-1}. They showed a fluctuating increasing trend from May 2017 to May 2018, and the values were relatively high and stable from September 2018 to April 2019. The concentrations of groundwater NO_2^--N ranged from 0.01 to 0.52 mg L^{-1}, and they were higher from May to October than in other months for both 2017 and 2018. Comparing the three inorganic forms of N, the concentrations of groundwater NO_3^--N were the highest, while NO_2^--N was the lowest among them. Overall, all three forms of groundwater inorganic N in the second year were generally higher than in the first year (Fig. 2d–f). This increase in annual NO_3^--N indicates that the shallow groundwater system might not be able to rapidly recover from N pollution.

300 The spatial variations of inorganic N concentrations in groundwater at the 14 sampling
301 sites are shown in Fig. 3 a–f. The GW-NO_3^--N concentrations were high and followed the
302 order of SG3, SG4, SG6, SG7, and SG2, while they were lower at the other sites.
303 Groundwater NH_4^+-N concentrations were the highest at SG3, followed by SG2, SG7.
304 Groundwater NO_2^--N concentrations were the highest at SG6, followed by SG4, SG5, SG7.
305 Overall, all the forms of groundwater inorganic N concentrations varied spatially in the
306 study area. Among them, the spatial variations of GW-NO_3^--N concentrations were highly
307 variable in the study area. Site SG1 showed the lowest GW-Dep and low GW-NO_3^--N
308 concentrations (Table 1). This is likely because the soil NO_3^--N source was lost by
309 denitrification under intermittent ponding irrigation during the summer rice season. Thus,
310 the NO_3^--N leaching was reduced at SG1. Compared with sites SG8–SG14, the sites
311 SG2–SG4 and SG6–SG7 had lower GW-Dep and showed higher GW-NO_3^--N
312 concentrations (Table 1). This could be because NO_3^--N leaching decreased with the
313 increase of vadose zone thickness (Weitzman et al., 2022). Sites SG5 and SG8-SG14
314 showed similar GW-NO_3^--N concentrations but were characterized by different GW-Dep. It
315 indicates that in addition to N source and leaching, other groundwater environmental
316 factors might affect GW-NO_3^--N. Overall, for the GW-NO_3^--N concentrations, about 24%
317 of samples exceeded the World Health Organization (WHO)'s water quality standard of 10
318 mg L^{-1}.

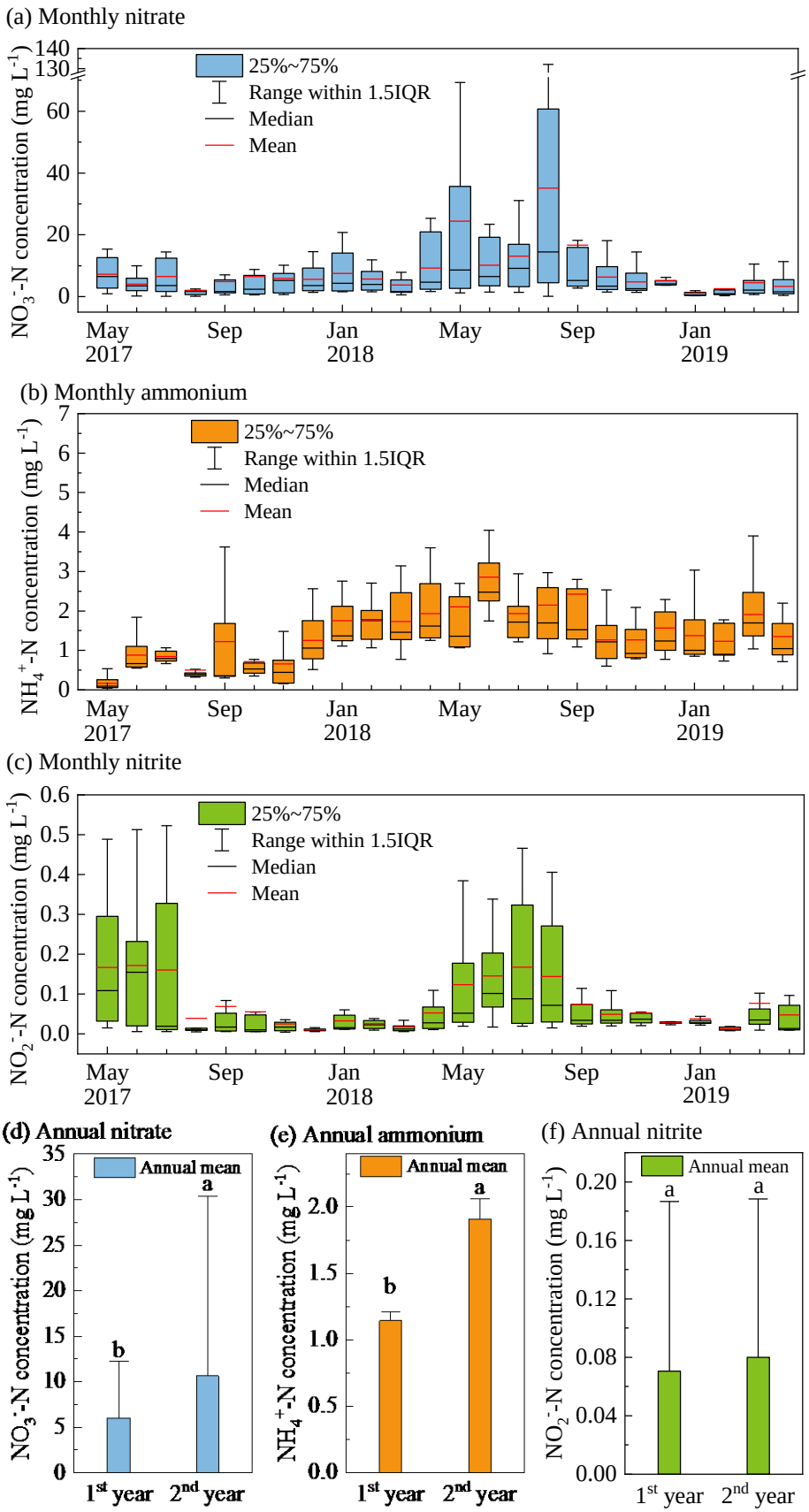

Fig. 2 Temporal variations of concentrations of (a) monthly nitrate, (b) monthly ammonium, (c) monthly nitrite, (d) annual nitrate, (e) annual ammonium, and (f) annual nitrite in groundwater. The different letters above the error bars in (d), (e), and (f) indicate significant difference ($p<0.05$) between the different years.

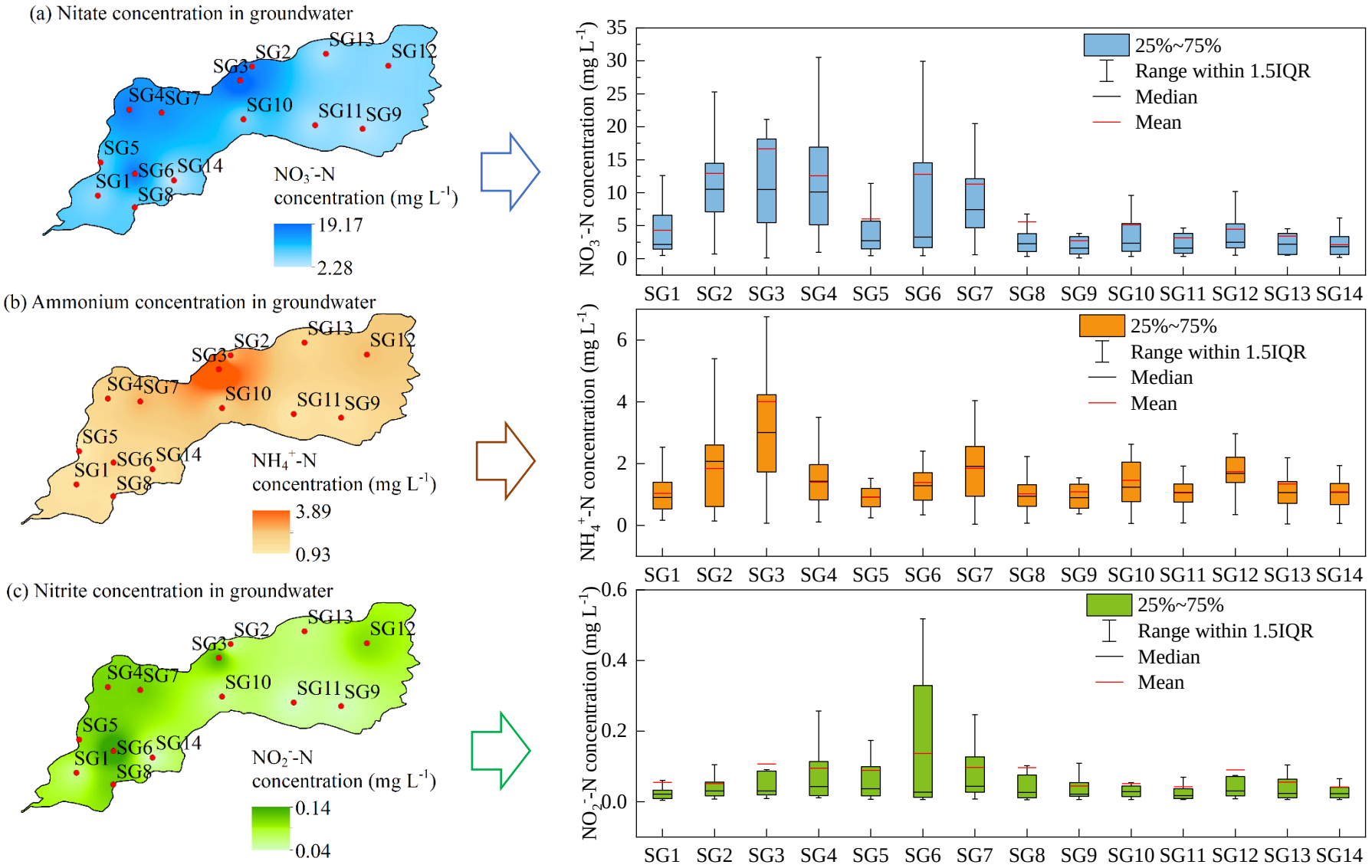

Fig. 3 Spatial distribution of concentrations of (a) nitrate, (b) ammonium, and (c) nitrite in groundwater

3.3. Spatiotemporal variations of groundwater nitrate isotopes

The δ^{15}N-NO_3^- values ranged from -20.16‰ to 107.88‰ with a mean value of 11.16±16.30‰. The δ^{18}O-NO_3^- values ranged from -15.69‰ to 56.56‰ with a mean value of 8.39±12.40‰. The temporal variations of the δ^{15}N-NO_3^- and δ^{18}O-NO_3^- values in groundwater from August 2018 to April 2019 are shown in Fig. 4a. The δ^{15}N-NO_3^- and δ^{18}O-NO_3^- values showed similar temporal variation trends. Groundwater NO_3^--N in August was heavily affected by leaching because of the application of fertilizer and manure and wheat residue return to the field in the wet season when heavy and high-frequency precipitation happens. Meanwhile, in the following months (September to April of the following year), the leaching amount was reduced due to less precipitation in the dry seasons. The measured mean δ^{15}N-NO_3^- value was 26.36‰ in August 2018, and the mean δ^{18}O-NO_3^- value was 17.83‰ in the same month. While the mean δ^{15}N-NO_3^- values ranged from 3.54‰ to 19.73‰ and the mean δ^{18}O-NO_3^- values ranged 2.91‰ to 10.79‰ from September 2018 to April 2019, both are lower than the measured values obtained in August 2018. During the periods August–October 2018, December 2018–January 2019, and March–April 2019, the δ^{15}N-NO_3^- and δ^{18}O-NO_3^- showed decreasing trends. The slight increase in the δ^{15}N-NO_3^- and δ^{18}O-NO_3^- values after October 2018 (during wheat sowing) and February 2019 (during wheat regeneration) can be attributed to the application of fertilizer, crop residue returning to the field, and irrigation. These management practices caused an increase in NO_3^--N denitrification rates due to the increase of soil NO_3^--N,

soil water, and organic carbon in the vadose zone.

The spatial distribution of the δ^{15}N-NO_3^- and δ^{18}O-NO_3^- values in groundwater are shown in Fig. 4b–c. The δ^{15}N-NO_3^- values from the SG5 (mean value of 29.55‰) were obviously higher than those of the other sites (mean values ranged from 0.92‰ to 14.35‰) (Fig. 4d). The maximum δ^{15}N-NO_3^- value of 107.88 ‰ was observed in August 2018 at SG5. This could be because the silt loam soil could have preserved soil water, and the manure application could have provided a carbon source for denitrification during wet season. Thus, the NO_3^--N denitrification rates could be higher during NO_3^--N leaching in the vadose zone at this silt loam site during the late wet season of August. Meanwhile, the δ^{18}O-NO_3^- values from the SG5, SG6, SG9, and SG14 (mean values ranged from 13.97‰ to 18.03‰) were higher than those of the other sites (mean values ranged from 2.05‰ to 8.67‰). At these sites, the δ^{18}O-NO_3^- values were as high as 33.93‰ to 50.69‰ in August 2018, indicating that NO_3^--N in precipitation was a direct source of recharge to the groundwater. This agrees well with the measured δ^{18}O-NO_3^- values in precipitation which ranged from 35‰–59‰ (VSMOW) as reported by Spoelstra et al. (2001).

(a) Temporal variations of stable isotopes of nitrate

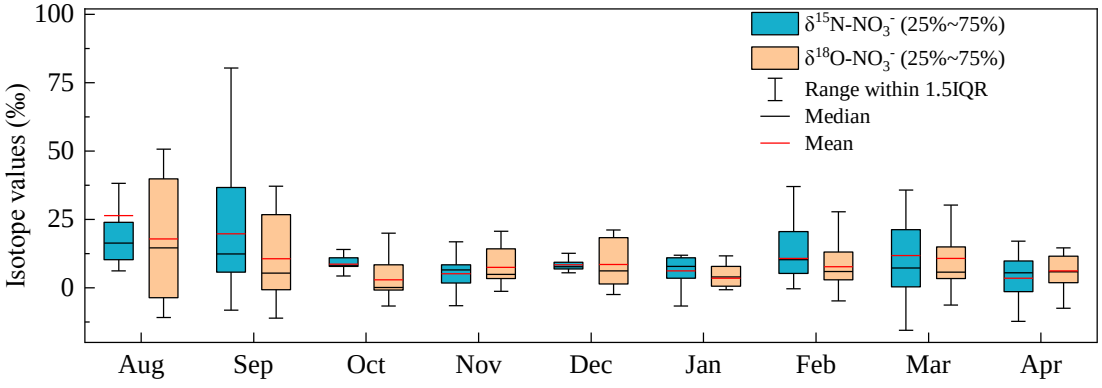

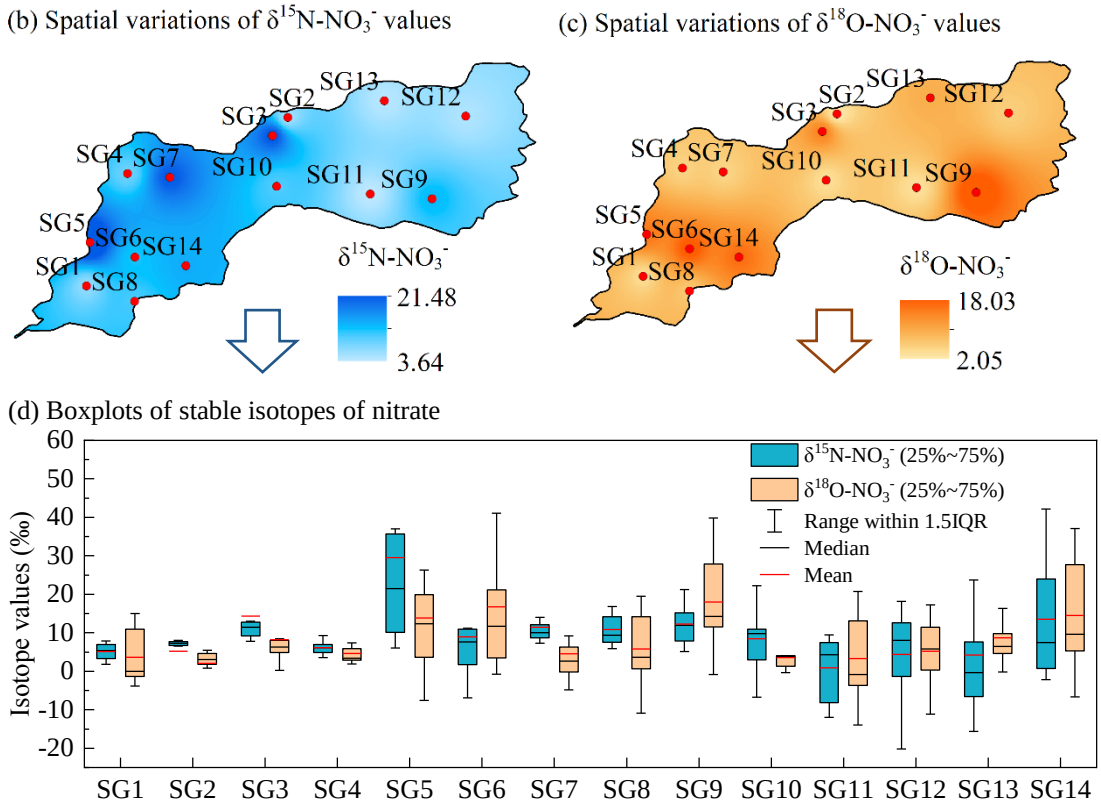

371

372

373 Fig. 4 (a) temporal variations of $\delta^{15}N\text{-}NO_3^-$ and $\delta^{18}O\text{-}NO_3^-$values, spatial variations of (b) $\delta^{15}N\text{-}NO_3^-$
374 and (c) $\delta^{18}O\text{-}NO_3^-$ values, and (d) box plots of $\delta^{15}N\text{-}NO_3^-$ and $\delta^{18}O\text{-}NO_3^-$ values at 14 sampling sites

375 *3.4. Prediction of spatiotemporal variations of groundwater nitrate*

376 In this study, the 19 effect factors in Table 2 were set as predictor variables, and
377 $GW\text{-}NO_3^-N$ was set as a response variable when applying random forest model. Fig. 5
378 shows the comparison between the measured and random forest model predicted
379 $GW\text{-}NO_3^-N$ for the training dataset and test dataset. For the training dataset, the
380 simulation results yielded an R^2 of 0.93, an RMSE of 4.94, and an MAE of 2.10. After
381 training, the model was validated using the test dataset, which yielded an R^2 of 0.92, an
382 RMSE of 3.87, and an MAE of 2.89, indicating that the model simulation results were
383 good. Compared with previous results from random forest models reported by
384 Ouedraogo et al. (2019), Pennino et al. (2020) and He et al. (2022), the model

385 constructed in this study achieved better performance in predicting NO_3^--N
386 concentrations in groundwater. In addition, the result of this study showed better model
387 accuracy (R^2 range of 0.92–0.93) compared to the studies of Knoll et al. (2019) and El
388 Amri et al. (2022), which used other machine learning models,e.g., classification and
389 regression trees and artifcial neural network, to assess groundwater NO_3^--N and yielded
390 a model accuracy (R^2) range of 0.39–0.90.

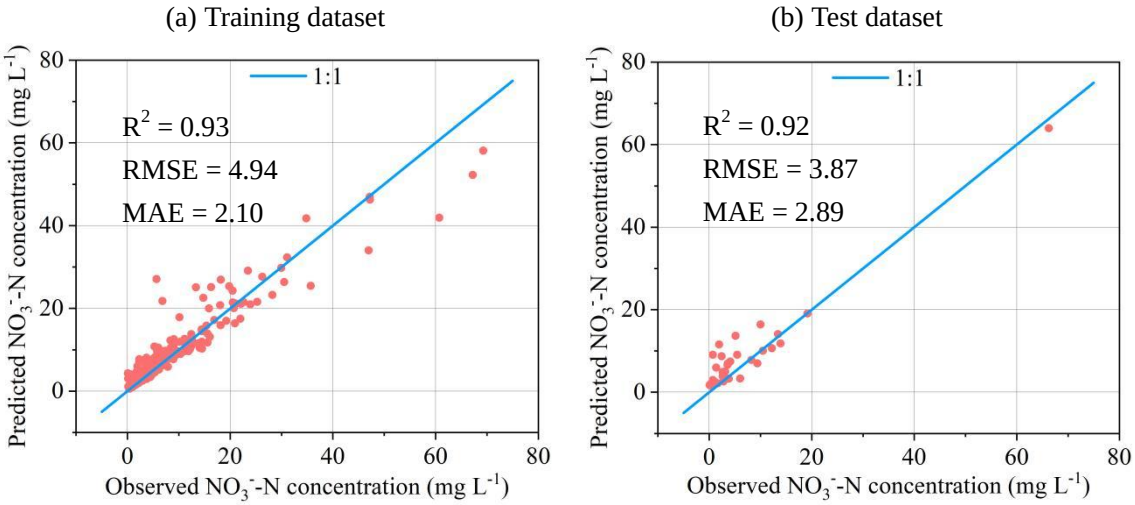

391 **Fig. 5** Comparison between the observed and random forest model predicted groundwater nitrate
392 concentrations in groundwater for the (a) training and (b) test datasets

393 The spatial and temporal distribution of the observed and random forest model
394 predicted groundwater NO_3^--N concentrations are shown in Fig. 6. Comparing the
395 measured and predicted spatial and temporal distributions of groundwater NO_3^--N
396 concentrations, the results showed that the predicted values were generally close to the
397 measured values. Despite its remarkable performance, the random forest model may
398 result in a loss when predicting the extreme ends or responses beyond the boundaries of
399 the training data (Smarra et al., 2018). Therefore, predicting values beyond the range in
400 the training data is not recommended. A representative training dataset is important for

assuring model performance when constructing a random forest model. In addition, it was found that the performance of the model may be influenced by other factors, such as the choice of a dependent variable, and independent variables, and the size of the dataset.

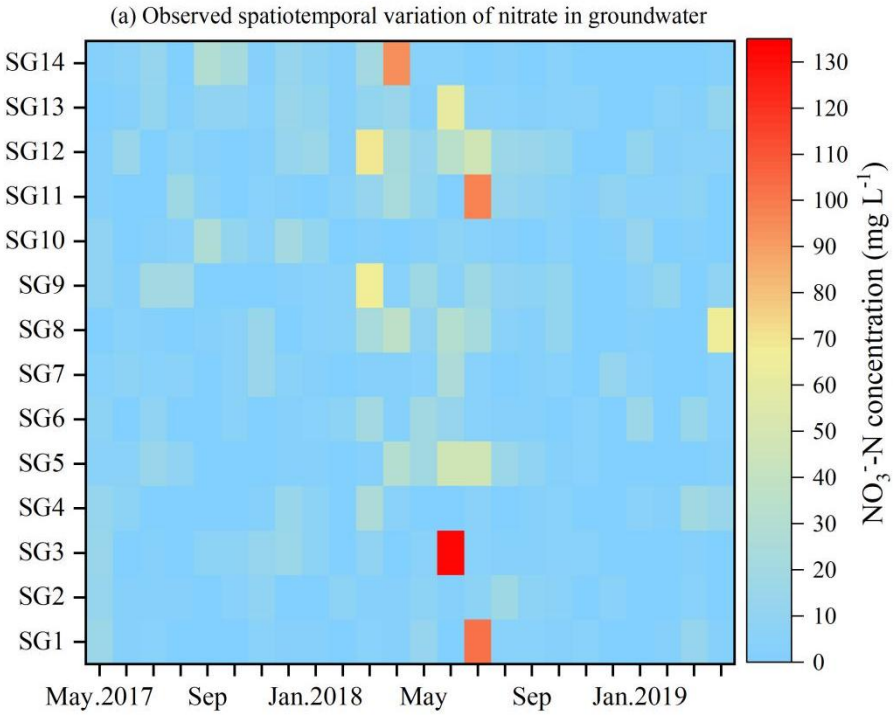

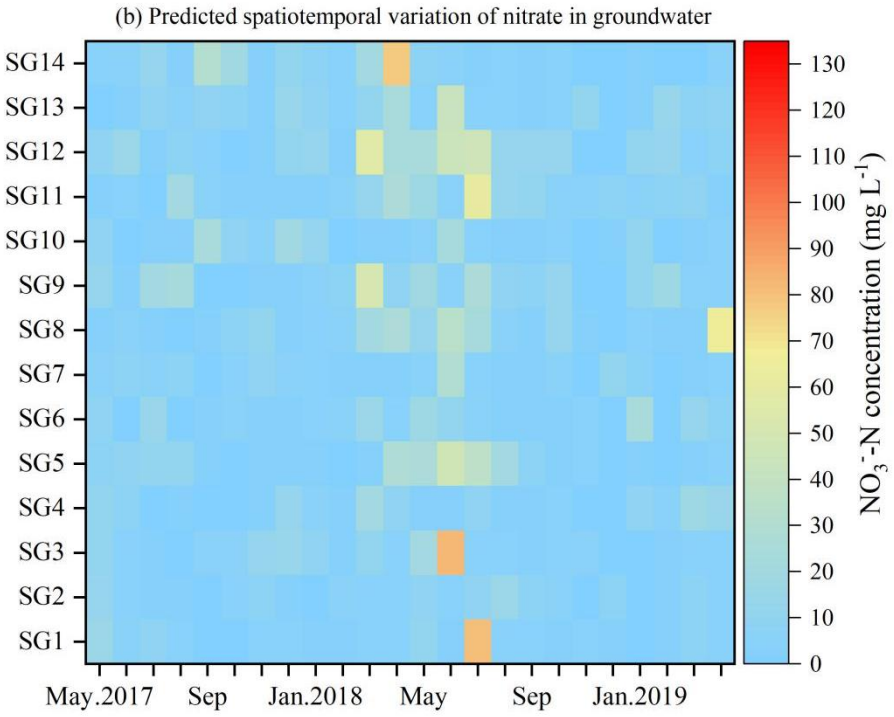

Fig. 6 Comparison between (a) observed and (b) the random forest model predicted spatiotemporal variation of nitrate in groundwater

3.5. Importance of effect factors on spatiotemporal variations of groundwater nitrate

The random forest importance and partial dependency analysis were used to calculate the importance of each influential factor on the spatiotemporal variations of GW-NO_3^--N, and to comprehensively analyze the relationship between environmental factors and GW-NO_3^--N (Figs. 7–8). As shown in Fig. 7, the key factors affecting GW-NO_3^--N concentrations were GW-NO_2^--N, GW-NH_4^+-N, S-SON, and GW-Dep, with relative importance of 21.46%, 6.92%, 6.91%, and 6.01%, respectively, which are all higher than 5.0%. Meanwhile the relative importance of the other factors to GW-NO_3^--N concentrations were all less than 5.0%. The GW-DON as the substrate of mineralization contributed an importance of 3.83%, which was less important than GW-NO_2^--N and GW-NH_4^+-N. Among the different surface soil N species, SON was the main influential factor on GW-NO_3^--N, followed by the S-NH_4^+-N (3.32%) and S-NO_3^--N (0.69%), whereas the importance of S-NO_2^--N (0.13%) was the smallest. The

GW-Dep impacted the leaching of N out of the vadose zone. Moreover, the SOC, SWC, and SSC also influenced GW-NO_3^--N with a relative importance of 4.19%, 2.56%, and 1.13%, respectively. Precipitation and irrigation were identified with a contribution of 3.96% and 1.45%, respectively. As for groundwater environmental factors influencing N transformation by changing microbial survival, GW-Temp was identified with a relative importance of 4.53%. Finally, the relative importance of the other factors yielded the following order GW-TDS (2.90%), GW-ORP (2.59%), GW-DO (1.71%), GW-DOC (1.12%), and GW-pH (0.96%). The relationships between the effect factors and groundwater NO_3^--N were further analyzed and are shown in Fig. 8 according to their order of importance.

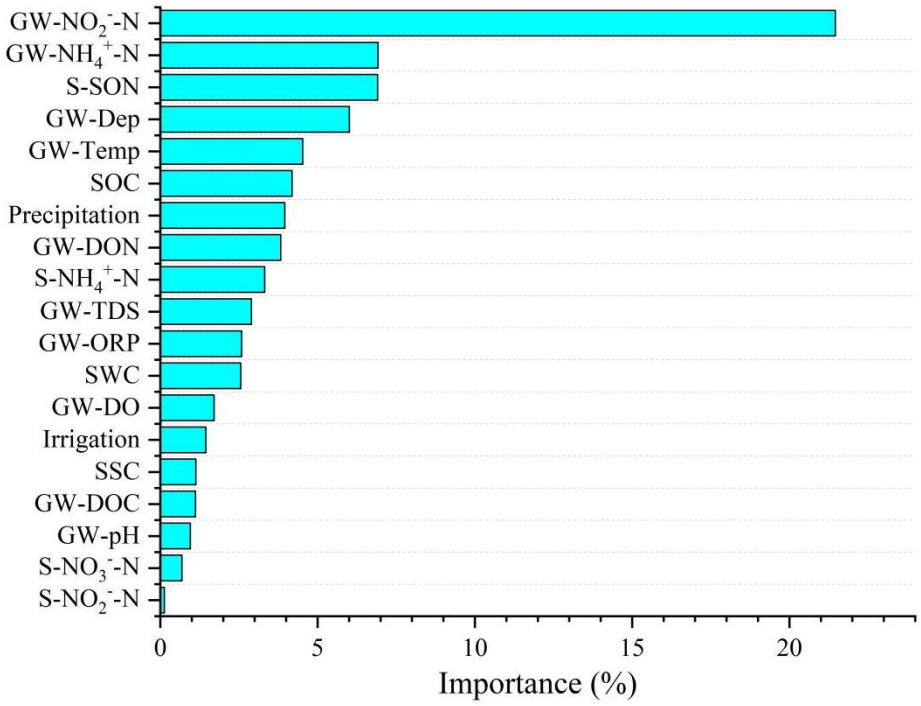

Fig. 7 Relative importance of potential effect factors to groundwater nitrate concentrations

3.6. Relationship between effect factors and groundwater nitrate

The relationships between the observed mean values of each explanatory variable, i.e., each effect factor (Table 2) and GW-NO_3^--N at the 14 sites are shown in Fig. S1 in the supporting information. Significant correlations were found between GW-NO_2^--N and

439 GW-NO_3^--N (r=0.84, p<0.01), between GW-NH_4^+-N and GW-NO_3^--N (r=0.59, p<0.05),
440 between GW-Dep and GW-NO_3^--N (r=-0.68, p<0.01), between GW-TDS and and
441 GW-NO_3^--N (r=0.56, p<0.05), and between GW-ORP and GW-NO_3^--N (r=0.57,
442 p<0.05). However, the interactions of all the effect factors resulted in nonsignificant
443 correlations between other factors and GW-NO_3^--N, and led to difficulty in reflecting
444 their impacts on groundwater NO_3^--N concentrations. Therefore, the partial dependence
445 plots based on the random forest model were used to show the complex nonlinear
446 relationships between GW-NO_3^--N and each effect factor, along with the frequency
447 distribution (Fig. 8a–s).

448 *3.6.1 Different forms of N in groundwater*

449 The GW-NO_2^--N and GW-NH_4^+-N were significantly positively correlated with the
450 GW-NO_3^--N, with an r of 0.92 (p<0.01) and 0.56 (p<0.01), respectively (Fig. 8a–b). A
451 positive correlation (r = 0.42, p<0.01) was identified between GW-DON and
452 GW-NO_3^--N (Fig. 5h). However, a negative correlation was found when DON was
453 below 100 mg L^{-1}. The GW-NO_2^--N, an intermediate product of nitrification and
454 denitrification, is of great importance in the N transformation process and is the most
455 crucial factor as an indicator of the NO_3^--N transformation rate. In this study, the
456 presence or accumulation of NO_2^--N showed the highest impacts on groundwater
457 NO_3^--N concentrations compared to the other factors (Fig. 7). This could be due to
458 denitrification as a heterotrophic process. The previous results of Du et al. (2016)
459 indicated that denitrifying bacteria in the system preferred using NO_3^--N as an electron
460 acceptor rather than NO_2^--N. Thus, the accumulation and production of NO_2^--N can
461 occur during denitrification, and NO_2^--N could be regarded as an index of the activity of
462 denitrifying bacteria. The high-throughput sequencing analysis of Du et al. (2016)

463 revealed that the genus of Thauera bacteria was dominant in the denitrifying community
464 with high NO_2^--N accumulation. According to the previous study, the DON retained by
465 the soil accounts for 25%-35% of the total DON, and the remaining amount enters the
466 groundwater with leaching (Zhou et al., 2003). The leached DON undergoes
467 mineralization (ammonification and nitrification) and subsequently causes an increase of
468 both NH_4^+-N and NO_3^--N in groundwater (Liu et al., 2022). The GW-DON can produce
469 GW-NH_4^+-N through ammonification and then indirectly influence GW-NO_3^--N
470 through nitrification of GW-NH_4^+-N (Wang et al., 2020; Liu et al., 2022). In this study,
471 the GW-NH_4^+-N was the second important factor influencing GW-NO_3^--N. This could
472 be due to the nitrification processes, where the GW-NH_4^+-N are the substrates for
473 NO_3^--N production by the nitrification process. During the nitrification processes,
474 because the oxidation of NO_2^--N to NO_3^--N is rapid in natural systems, the slower
475 oxidation of NH_4^+-N to NO_2^--N is the main process that controls NO_2^--N production
476 (Nikolenko et al., 2018). Both NO_3^--N and NO_2^--N appeared when organic N
477 mineralization occurred in groundwater. The GW-NH_4^+-N showed higher importance
478 and a greater correlation coefficient than GW-DON, which might indicate that NH_4^+-N
479 can be rapidly converted into NO_3^--N. Thus, it is likely that the GW-NO_2^--N is an
480 intermediate product of denitrification in this study. Overall, the availability of
481 GW-NO_2^--N and GW-NH_4^+-N are indicated them as the primary factors reflecting the
482 denitrification and nitrification rates. Their highly ranked importance showed clear
483 evidence that N transformation played a critical role in controlling groundwater NO_3^--N
484 variations.

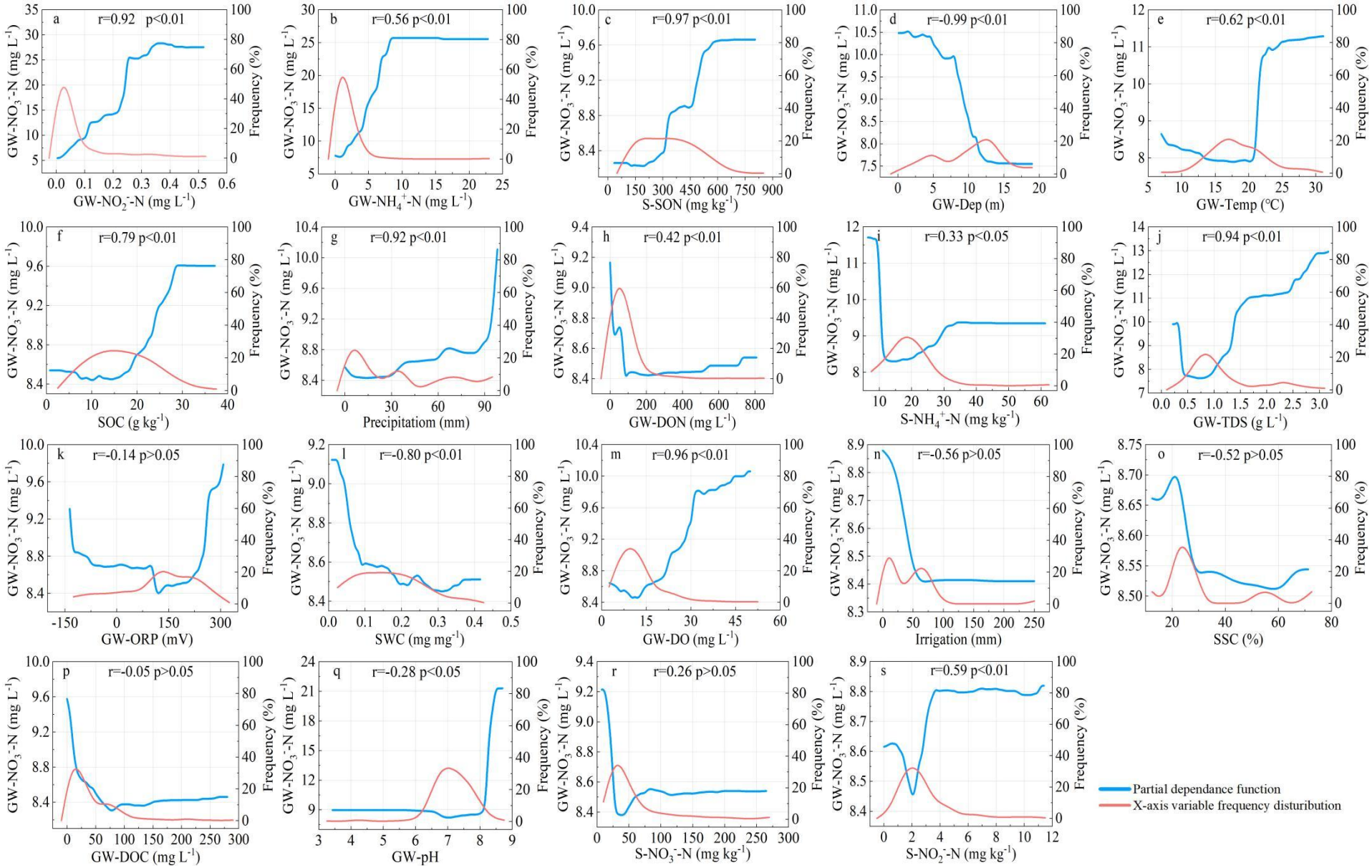

Fig. 8 Partial dependence plots of constructed random forest model. Blue lines show the partial dependence function, and red lines show the x-axis factor frequency

3.6.2 Different forms of N in surface soil and vadose zone characteristics

The spatiotemporal variations of GW-NO_3^--N depended on different forms of N content in the soil and leaching. In terms of N forms in the soil, there are positive correlations bwtween SON and GW-NO_3^--N ($r = 0.97$, $p<0.01$, Fig. 8c), bwtween S-NO_2^--N and GW-NO_3^--N ($r = 0.59$, $p<0.01$, Fig. 8s), and bwtween S-NH_4^+-N and GW-NO_3^--N ($r = 0.33$, $p<0.05$, Fig. 8i). This is mainly because mineralization and nitrification play critical roles in the production of NO_3^--N and the subsequent NO_3^--N leaching. Moreover, a higher S-SON might indicate more accumulated organic and inorganic N in the vadose zone. On the other hand, another possible explanation is that the soil-leached SON, NH_4^+-N, and NO_2^--N has undergone a transformation and produced NO_3^--N in the vadose zone before entering into the groundwater. Despite the fact that S-NO_3^--N has a direct impact on GW-NO_3^--N, no significant correlation was found between them ($r = 0.26$, $p>0.01$) (Fig. 8r). The S-NO_3^--N could be divided into two groups by the threshold around 30 mg kg^{-1}. A negative correlation was found when S-NO_3^--N was below 30 mg kg^{-1}, indicating that the lower S-NO_3^--N could be attributed to more NO_3^--N leaching loss. In contrast, their relationship changed to be positive when S-NO_3^--N was above 30 mg kg^{-1}, indicating that more NO_3^--N in surface soil resulted in more NO_3^--N leaching loss into the groundwater.

The depth from the soil surface to the groundwater table plays an essential role in the accumulation and reduction of N leaching loss in the vadose zone. The GW-Dep was significantly negatively correlated with the GW-NO_3^--N ($r = -0.99$, $p<0.01$) (Fig. 8d). Our results showed that a shallower groundwater table leads to an increasing amount of NO_3^--N in groundwater, consistent with many previous studies (Awais et al., 2021; Li et al., 2021; El Amri et al., 2022; He et al., 2022). Other characteristics of the vadose zone also affected N transformation and subsequent

leaching of NO_3^--N, including SWC, SSC, and SOC. A significant negative correlation ($r = -0.80$, $p<0.01$) was found between SWC and GW-NO_3^--N (Fig. 8l). The increase of SWC caused the decrease of NO_3^--N production by nitrification and enhanced denitrification removal of NO_3^--N in the soil (Sexstone et al., 1985). However, it is notable that a positive correlation was identified when the SWC was above 0.30. This could be because higher SWC increases NO_3^--N leaching into the groundwater. No significant negative correlation ($r = -0.56$, $p>0.05$) was found between irrigation and GW-NO_3^--N (Fig. 8n). Meanwhile, a significant positive correlation ($r = 0.92$, $p<0.01$) was identified between precipitation and GW-NO_3^--N (Fig. 8g). Irrigation and precipitation influenced both soil water content and soil water percolation. Irrigation mainly results in the increase of SWC but might not increase N leaching loss because the higher SWC could enhance the denitrification rate, which reduces NO_3^--N content in root zone soil (Sexstone et al., 1985). However, precipitation is more likely to increase soil-soluble N leaching into the groundwater due to the increase of antecedent SWC by irrigation (Razzaghi et al., 2012). Thus, precipitation exhibited higher importance than irrigation and SWC, as shown in Fig. 7. No significant correlation ($p>0.05$) was observed between SSC and GW-NO_3^--N (Fig. 8o). However, it should be noted that when SSC is around 20%, the GW-NO_3^--N was obviously higher; that is, the GW-NO_3^--N decreased with SSC when the SSC was less than 60%. In contrast, the GW-NO_3^--N showed a slight increase when the SSC was higher than 60%. The SSC can influence SWC and the subsequent N leaching in soil. Less sand content might be associated with higher antecedent SWC and more preferential flow (Van Es et al., 2004; Razzaghi et al., 2012). Thus, the N leaching might be increase with the decrease of SSC. On the other hand, the nitrification rate increased when the SSC was higher than 60% in sandy loam soil. Thus, the soil

NO_3^--N content and leaching correspondingly increased. A significant positive correlation ($r = 0.79$, $p < 0.01$) was identified between SOC and GW-NO_3^--N (Fig. 8f). This could be due to the higher SOC, which usually associated with higher SON in soil and corresponds to more N leaching. Nevertheless, when SOC was below 15 g kg^{-1}, it had a minor impact on GW-NO_3^--N.

3.6.3 Groundwater environmental conditions

The DO and ORP are indicators of redox status in the groundwater environment. In this study, DO usually ranged from 4 to 20 mg L^{-1}. It is generally believed that the appropriate DO concentration for denitrification is 2 mg L^{-1} (Peng et al., 2020). Denitrification still exists when the DO concentration of groundwater is 2~6 mg L^{-1}, but the rate is reduced with higher DO (Peng et al., 2020). The average monthly DO concentration in the study area from May 2017 to April 2019 was 11.78 mg L^{-1}, and there was no record of below 2 mg L^{-1} values in any of the samples. Instead, the DO values in 14.6% of the 336 samples were between about 2 and 6 mg L^{-1}, mainly in April and August–October. Overall, a significant positive correlation ($r = 0.96$, $p<0.01$) was identified between GW-DO and GW-NO_3^--N (Fig. 8m), which could be due to nitrification. Meanwhile a negative correlation was identified when DO was less than 10 mg L^{-1} (Fig. 8m). This could be due to stronger denitrification than nitrification. An increase of GW-NO_3^--N with ORP is observed when ORP is above 200 mV. This could be due to the positive correlation between ORP and actual nitrification (Bohrerova et al., 2004). No significant correlation ($p>0.05$) was found between GW-ORP and GW-NO_3^--N (Fig. 8k). When ORP was less than -100 mV, it is notable that there was a negative correlation, while a positive correlation was identified when ORP was great than 100 mV. Nevertheless, when the ORP was between -100 mV and 100 mV, it had a minor impact on GW-NO_3^--N. According to

565 the relationships between GW-NO_3^--N and DO and between GW-NO_3^--N and ORP
566 based on the partial dependence plots of the random forest model (Fig. 8), the
567 environment of groundwater can be classified as being under nitrate-reducing
568 conditions if the DO is less than 10 mg L^{-1} and the ORP is less than -100 mV. On the
569 other hand, the groundwater environment can be described as being and under
570 nonreducing conditions if the DO is greater than 10 mg L^{-1} and the ORP is greater
571 than 100 mV. This is in accordance with previous studies (Rivett et al., 2008; Jahangir
572 et al., 2017; Thayalakumaran et al., 2008). Groundwater DO and ORP are shown to
573 be pH dependent. Thus, the nitrification and denitrification rates could vary with
574 changes in pH (Bohrerova et al., 2004). The GW-pH showed a significantly negative
575 correlation with GW-NO_3^--N ($r = -0.28$, $p<0.05$) (Fig. 8q). The groundwater NO_3^--N
576 decreased with an increasing trend of pH from 6.0 to 7.0, which could be attributed to
577 denitrification. Meanwhile groundwater NO_3^--N increased with pH from 7.0 to 8.0,
578 which could be attributed to nitrification. The results of this study are consistent with
579 previous studies, which reported that the highest denitrification removal of NO_3^--N
580 was at a pH of 6.0–7.5 and the most adapted pH range for nitrifying bacteria is 7.0 to
581 9.0 (Ghafari et al., 2009; Hu et al., 2018; Bergamasco et al., 2019). A drastic increase
582 of NO_3^--N is observed when pH was above 8.0. This could be attributed to soil water
583 percolation to shallow groundwater following fertilization and irrigation during the
584 rainy season (Jendia et al., 2020).

585 The DOC is considered as the source of electron donors for denitrification
586 (Thayalakumaran et al., 2008). Overall, there was no significant correlation ($r = -0.05$,
587 $p>0.05$) observed between GW-DOC and GW-NO_3^--N (Fig. 8p). A negative
588 correlation was found when DOC was below 75 mg L^{-1}, while a positive correlation
589 was found when DOC was above 75 mg L^{-1}. A concentration value of DOC > 1.0 mg

590 L^{-1} can indicate the presence of electron donors significant enough to support
591 denitrification (Rivett et al., 2008; Thayalakumaran et al., 2008). The DOC
592 concentrations of the 336 samples observed in this study ranged from 0.42 to 280.26
593 mg L^{-1}, with more than 99% of samples exceeding 1.0 mg L^{-1}. The negative
594 relationship between GW-NO_3^--N and DOC indicates the role of DOC as a carbon
595 source in the reduction processes (Rivas et al., 2017). The other electron donors, such
596 as Fe^{2+}, Mn^{2+}, and S^{2-}, might also exist in groundwater and influence N
597 transformation, but their roles are not dependent on temperature, DO, and ORP (Pang
598 and Wang, 2021). A significant positive correlation ($r = 0.94$, $p<0.01$) was found
599 between GW-TDS and GW-NO_3^--N (Fig. 8j). The GW-TDS was usually higher than
600 0.5 g L^{-1}; however, when it was lower than this value, there was a negative correlation
601 between them. The other electron donors, rather than DOC, might have played critical
602 roles when TDS was below 0.50 g L^{-1}, causing the negative correlation between
603 GW-NO_3^--N and TDS. However, when it was higher than 0.5 g L^{-1}, a positive
604 correlation was found between NO_3^--N and TDS. This could be because the growth of
605 denitrification bacteria is reduced with the increase of salinity. A previous study
606 reported that denitrification was more sensitive to salt compared to nitrification
607 (Dinçer and Kargi, 1999). Besides, it could also be because the groundwater TDS was
608 increased by a large amount of NO_3^--N leaching.

609 The groundwater temperature controls microbial activity. Overall, a positive
610 correlation ($r = 0.62$, $p<0.01$) was found between GW-Temp and GW-NO_3^--N (Fig.
611 8e), which could be due to higher N leaching to groundwater in the summer period.
612 When the GW-Temp was below 20℃, a negative correlation was found between
613 GW-Temp and GW-NO_3^--N. This could be because the increased temperature

enhances the growth and activity of denitrifiers, thus, reducing NO_3^--N in groundwater (Singh et al., 2010). The groundwater temperature also impacts other environmental factors, such as DO and DOC availability (Thayalakumaran et al., 2008; Nikolenko et al., 2018). The DOC can be stimulated, and the DO can be depleted by increased groundwater temperature (Guo et al., 2017). The suitable temperature for the nitrification rate is 10°C–35°C, with the optimum temperature ranging between 25°C–30°C (Hayatsu and Kosuge, 1993). In contrast, the suitable temperature for denitrification is 20°C–43°C (Strous et al., 1999). In general, higher temperatures result in stronger denitrification and nitrification activity in the groundwater environment with temperatures less than 25°C. The optimum temperature for denitrification is relatively higher than that for nitrification (Nikolenko et al., 2018).

Although the relative importance of groundwater environmental factors (i.e., temperature, DO, ORP, DOC, TDS, and pH) to groundwater NO_3^--N were less than 5.0% (Fig. 7), the partial dependence plots generated by the random forest model suggested that they play important roles in influencing nitrification and/or denitrification in groundwater (Fig. 8). The groundwater NO_3^--N, δ^{15}N-NO_3^- and δ^{18}O-NO_3^- exhibited tremendous changes in the summer periods in this study, probably due to simultaneous leaching and denitrification (Figs. 2–4). The nitrification rate also increases with an increase in temperature. In November, January, and February, when the temperature is low, the DO and ORP increase, and less DOC

635 is consumed, indicating a more oxidizing condition. During these months, denitrifying
636 bacteria growth might be limited by the low temperature (Nikolenko et al., 2018).
637 Thus, the denitrification is low, and nitrification might superimpose on denitrification
638 during these low-temperature periods.

639 *3.7. Identification of key N transformation processes in groundwater using isotopes*

640 The simultaneous increase of $\delta^{15}N\text{-}NO_3^-$ and $\delta^{18}O\text{-}NO_3^-$ with a slope of 0.5-1.0
641 ($\delta^{18}O/\delta^{15}N$) is attributed to denitrification (Osaka et al., 2010; Wells et al., 2016) (Fig.
642 9). If strong denitrification occurs in groundwater, the slope of the linear relationship
643 (k) between $\delta^{15}N\text{-}NO_3^-$ and $\delta^{18}O\text{-}NO_3^-$ is close to 0.5, and $\delta^{15}N\text{-}NO_3^-$ in groundwater is
644 significantly negatively correlated with $\ln[NO_3^-]$ (Zhang et al., 2019). Among the 14
645 observation sites in the study area, the linear relationship slope (k) of $\delta^{15}N\text{-}NO_3^-$ and
646 $\delta^{18}O\text{-}NO_3^-$ in 8 sites, that is, SG1 (k = 0.98, R^2 = 0.85), SG3 (k = 0.83, R^2 = 0.98),
647 SG4 (k = 0.50, R^2 = 0.047), SG6 (k = 0.87, R^2 = 0.87), SG8 (k = 0.81, R^2 = 0.12),
648 SG13 (k = 0.59, R^2 = 90), SG14 (k = 0.82, R^2 = 0.70), and SG11 (k = 1.05, R^2 = 0.50),
649 ranged from 0.5 to 1.0 and with high $\delta^{15}N\text{-}NO_3^-$ composition, strongly supporting the
650 occurrence of denitrification in the NO_3^--N source and/or transformation in
651 groundwater (Fig. 9). The k value at SG7 (0.30, R^2 = 0.64), SG5 (0.44, R^2 = 0.84),
652 and SG10 (0.34, R^2 = 0.22) did not fall into the denitrification line. However,
653 relatively higher $\delta^{15}N\text{-}NO_3^-$ and $\delta^{18}O\text{-}NO_3^-$ than the potential NO_3^--N sources
654 indicated that weak denitrification still existed. The $\delta^{15}N\text{-}NO_3^-$ and $\delta^{18}O\text{-}NO_3^-$ at SG1,
655 SG4, SG10, SG11, and SG12 were relatively smaller, indicating weaker
656 denitrification. In this study, the groundwater $\delta^{15}N\text{-}NO_3^-$ was barely found to be
657 negatively correlated with $\ln[NO_3^-]$. It is likely that the isotopic fingerprint of
658 denitrification was simply masked by the pulse inputs of leached NO_3^--N from the

vadose zone. In addition, it might also be because shallower groundwater has a short residence time. Thus, transport of NO_3^--N affects the isotopic fingerprint of denitrification.

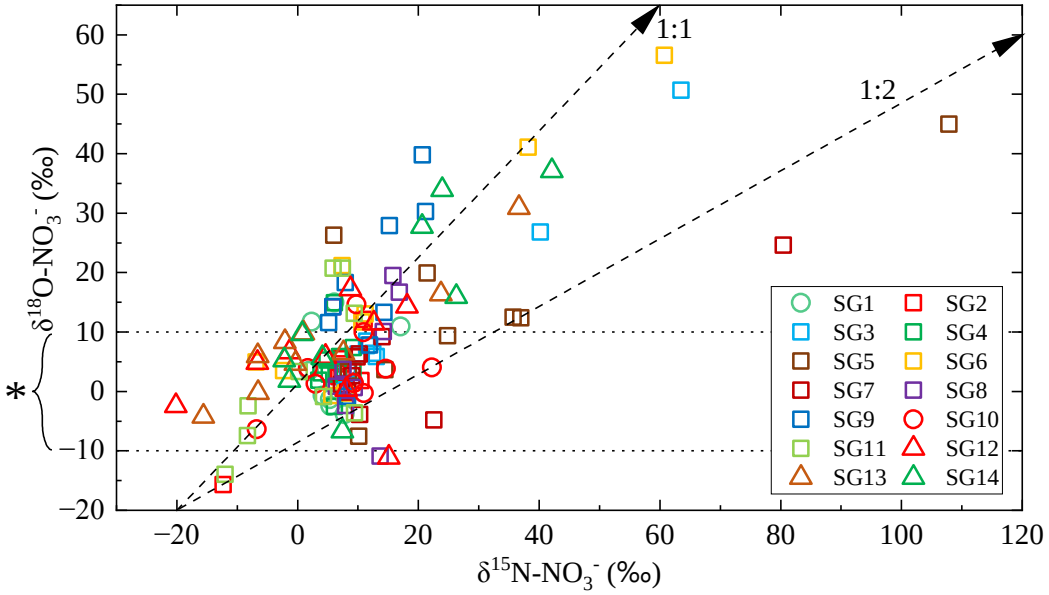

Fig. 9. Relationship between δ^{15}N-NO_3^- and δ^{18}O-NO_3^- in groundwater (the * indicates the range of nitrified δ^{18}O-NO_3^- within the dotted line, the 1:2 broken line indicates strong denitrification, and the 1:1 broken line indicates nitrification and denitrification)

Nitrification will simultaneously increase NO_3^--N concentrations and reduce the abundance of δ^{15}N-NO_3^- due to the isotope fractionation. The δ^{15}N-NO_3^- and δ^{18}O-NO_3^- vary along the 1:1 line and, with an R^2 closer to 1, indicates that the nitrification occurred concurrently with denitrification (Fig. 9). Moreover, nitrification in the groundwater environment resulted in the final δ^{18}O-NO_3^- values being mostly between -10‰ and 10‰ (Xue et al., 2009; Ji et al., 2021). In this study, the δ^{18}O-NO_3^- values of 64.28‰ of the 182 measured data were between -10‰ and 10‰, indicating that nitrification also existed in the shallow groundwater of the study area. The NO_3^--N is expected to be mainly from nitrifying processes since δ^{18}O-NO_3^- values in 80% of the samples the ranged from −5‰ to 5‰, which is fits within the range of -6.1‰–5.2‰ (Osaka et al., 2010). The relationship between the monthly

677 $\delta^{15}N\text{-}NO_3^-$ and NO_3^--N (from September 2018 to April 2019) in the 14 sites is shown
678 in Fig. 10. Nitrification along the groundwater flow path was identified, including in
679 the flow path along L1 surrounded by sites SG5, SG7, SG3, and SG1 and in the flow
680 path L2 surrounded by sites SG8, SG10, SG11, SG12, and SG13 (Fig. 10). Data with
681 negative $\delta^{15}N\text{-}NO_3^-$ abundance in September 2018, January 2019, and April 2019
682 were excluded from SG11 because the site was irrigated and fertilized in those
683 months. The more negative $\delta^{15}N\text{-}NO_3^-$ and $\delta^{18}O\text{-}NO_3^-$ ranges measured fell within the
684 expected range for NO_3^--N produced from urea/urine (Wells et al., 2016). Wang et al.
685 (2020) has reported that nitrification occurred in the groundwater, which is consistent
686 with results of this study.
687 Along the groundwater flow path L1, nitrification increased NO_3^--N
688 concentrations by about 10 mg L^{-1}. Meanwhile along the groundwater flow path L2,
689 nitrification increased NO_3^--N concentrations by about 2 mg L^{-1}. Higher nitrification
690 rates along flow path L1 were observed. This is due to the shallower and decreased
691 depth of the groundwater table along the groundwater flow direction (from 9.37 to
692 3.86 m). On the other hand, along flow path L2, the depth of the groundwater table
693 increased from 2.0 to 14.8 m. The denitrification rates along flow path L1 were also
694 stronger, as evidenced by the higher $^{15}N\text{-}NO_3^-$ at sites around flow path L1. This is
695 because the temperature and contents of electron donors (DOC and TDS) at sites
696 around flow path L1 were higher than those around flow path L2. Therefore, both
697 denitrification and nitrification were higher in shallower groundwater around flow
698 path L1 than flow path L2. Overall, based on the DO, ORP, different forms of N
699 concentrations, and nitrate isotopic composition, it can be concluded that nitrification
700 occurred concurrently with denitrification in this shallow groundwater system. The

co-occurrence of denitrification and nitrification found in this study is consistent with the findings from a previous study by Osaka et al. (2010).

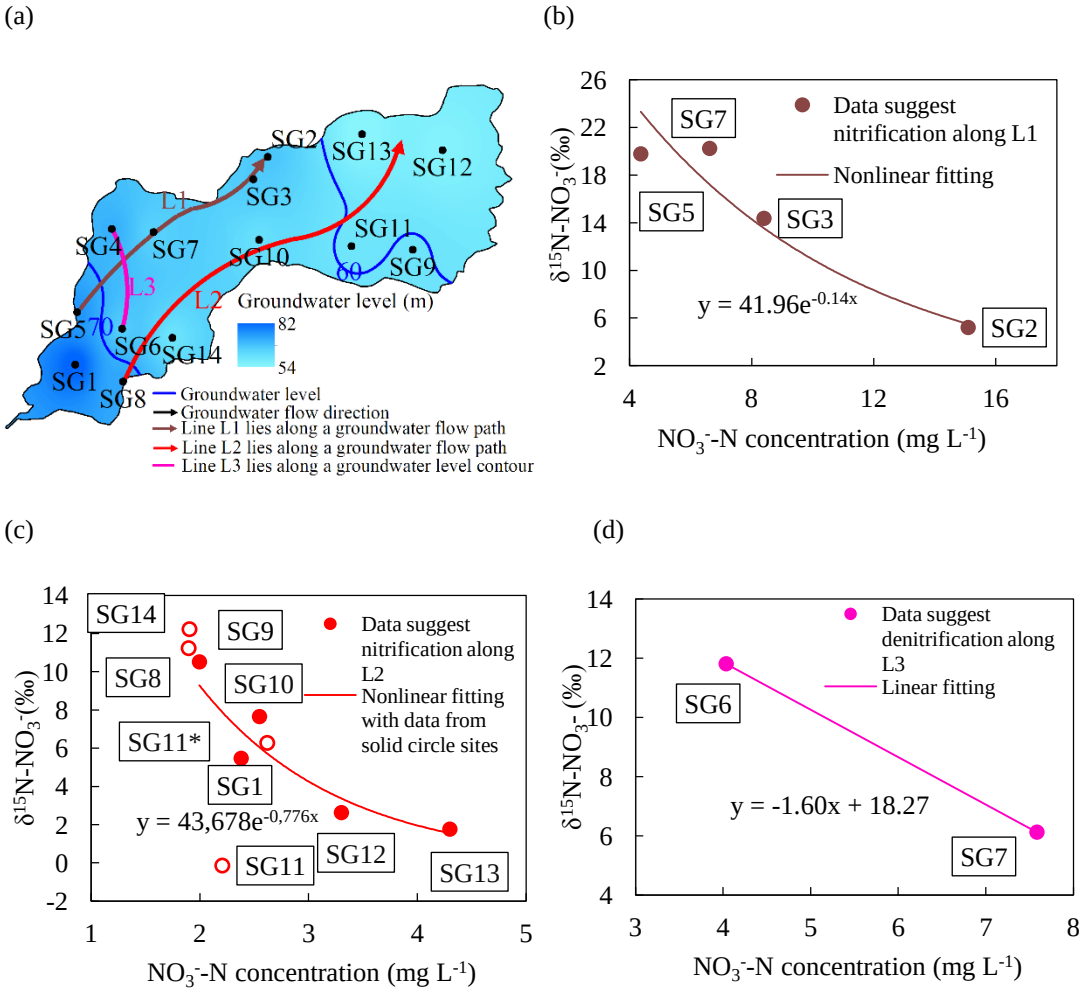

Fig. 10. (a) Locations of sampling sites along the groundwater flow path lines (L1 and L2) or the groundwater-level contour line (L3) and the relationship between monthly average (from September 2018–April 2019) groundwater $\delta^{15}N\text{-}NO_3^-$ and NO_3^--N concentrations at the 14 sampling sites along (b) L1, (c) L2, and (d) L3 (SG11*: data with negative $\delta^{15}N\text{-}NO_3^-$ abundance in September 2019, January 2019, and April 2019 were excluded from SG11)

Site SG1 was located upstream of groundwater flow with the shallowest depth of the groundwater table. However, NO_3^--N concentration at SG1 ranged between SG8 and SG12 as shown in Fig. 10.This is because the irrigation water source was from the Yellow River at SG1, while groundwater was abstracted for irrigation at other

716 sites. Moreover, the groundwater at SG1 might have received NO_3^--N from vertical
717 and lateral recharge of the Yellow River. It is notable, though, that the irrigation
718 schedule during the summer rice growth period at SG1 was different from that of the
719 other sites. High $\delta^{15}N\text{-}NO_3^-$ and low NO_3^- concentration values were found at SG14.
720 The groundwater table depth of SG14 was the deepest and was caused by
721 groundwater abstraction for paper production in factories, according to the Xinxiang
722 City Water Resources Bulletin in 2017 (XCWRB, 2017). The deep groundwater table
723 meant that NO_3^--N might have already been denitrified before arriving in the
724 groundwater (Vidon and Hill, 2004). As for SG9, there was a river nearby where
725 surface water could recharge the groundwater. The mean DO concentration was about
726 14.6 mg L^{-1} at SG9, while it ranged from 10.2 to 12.8 mg L^{-1} at the other sites. The
727 relatively higher DO at SG9 than the other sites could support the reasoning that
728 surface water existed recharge to the groundwater. The denitrification occurred
729 underneath the riverbed, and the denitrified NO_3^--N continuously flowed to the
730 groundwater at SG9. In addition, the DOC was lower at SG9 (41.9 mg L^{-1}) than at the
731 neighboring sites of SG11 (45.8 mg L^{-1}) and SG 12 (45.2 mg L^{-1}) because DOC was
732 consumed by denitrification underneath the riverbed. Therefore, the isotopic
733 composition and proportion of NO_3^--N sources at SG9 differed from that of the other
734 sites. The sites SG6 and SG4 near L3 in Fig. 10 lay along the groundwater water-level
735 contour line. The value of $\delta^{15}N\text{-}NO_3^-$ at SG6 was higher than that at SG4. The
736 groundwater table depth at SG6 was slightly higher than that of SG4. In addition, the
737 concentration of DOC in the groundwater of SG6 was higher than that at SG4.
738 Therefore, the stronger denitrification at SG6 could be attributed to the sufficient
739 carbon sources in the groundwater to support denitrification. Furthermore, the deeper

vadose zone thickness could provide enough time for denitrification before entering the groundwater.

4. Implications and Limitations

4.1. Groundwater nitrate pollution risk and attenuation in agricultural areas

The spatiotemporal variations of groundwater NO_3^--N concentrations can be explained by inorganic and organic N leaching and subsequent N transformation in groundwater. A shallower groundwater table is more vulnerable to N contamination. The deeper the vadose zone, the less likely contaminants are coming from leaching. However, continuous organic and inorganic fertilizer application under the combined effects of irrigation and precipitation can result in massive N accumulation in the deep vadose zone, and the peak of N content in soil contentiously moves downward to groundwater (Weitzman et al., 2022). The inorganic and organic N in groundwater located in a region with both a shallower groundwater table and high groundwater level can be transported to a lower groundwater water-level region. In addition, the groundwater is undergoing nitrification along the groundwater-level gradient. Thus, slow DON mineralization and nitrification might continuously increase NO_3^--N along the groundwater flow path, threatening groundwater quality for a long time. Therefore, the soil DON and NH_4^+-N leaching and the subsequent transformation in groundwater should not be overlooked when evaluating groundwater N pollution and making nonpoint source control policies. In our research, the groundwater flow could export the N out of the study area, thus, contributing to the temporal decrease of NO_3^--N in the local groundwater while also posing as a groundwater pollution threat to neighboring areas.

The rapid decrease of NO_3^--N during May–August indicated that the leached NO_3^--N was consumed immediately by denitrification. The temporal increases of

765 NO_3^--N were observed from September 2017 to January 2018 and from January 2019
766 to March 2019. In addition, the increase of NO_3^--N occurred along the groundwater
767 flow during September 2018–April 2019. These results suggested that the NO_3^--N
768 accumulation might occur under low groundwater temperature conditions. This is
769 mainly due to the denitrification rate decreasing at lower temperatures in groundwater
770 (Singh et al., 2010). Therefore, sufficient DOC must be provided for the efficient
771 removal of groundwater NO_3^--N when the groundwater temperature is suitable or
772 optimum for denitrification, particularly in late spring, summer, and early autumn. In
773 the future, quantifying nitrification and denitrification rates at different time scales
774 (e.g., daily, monthly, seasonally, or annually) is necessary to put forward N
775 attenuation measures. Agronomists recommend the application of organic fertilizer
776 and crop residue return with reduced chemical fertilizer in China and around the
777 world to increase soil quality (Zhao et al., 2016). Management of organic fertilizers
778 and crop residue is as crucial as chemical fertilizer application for reducing the risk of
779 SON accumulation and subsequent groundwater and surface water pollution while
780 providing enough DOC for denitrification. Furthermore, scientists and policy makers
781 should pay attention to the leaching risk of stocked N and evaluate its transport delay
782 time to protect groundwater quality in agricultural areas.

783 *4.2. Implications of groundwater nitrate prediction and limitations of this study*

784 The performance of the random forest model demonstrates that it can be well
785 applied for predicting spatial and intra-annual variations of groundwater nitrate
786 concentrations. The importance analysis for the influencing factors likewise provides
787 strong evidence for determining the main influencing factors and processes of NO_3^--N
788 in groundwater. In the NCP irrigation area, the effect of N transformation in

groundwater is as important as soil N leaching on the variations of NO_3^--N in shallow groundwater. The findings of this study can provide technical support for the rapid prediction and evaluation of N pollution in shallow groundwater through readily available effect factors at higher spatial and temporal resolution. The simplified approach of the random forest model can be applied in irrigation regions around the world to predict the spatial and temporal variations of NO_3^--N in groundwater. Unlike NO_3^--N, adsorption/desorption processes dominate DON and NH_4^+-N transport in the soil-groundwater systems (Vandenbruwane et al., 2007; Wang et al., 2021). Therefore, other factors related to adsorption/desorption processes are required to predict spatiotemporal variations of DON and NH_4^+-N concentrations in groundwater using machine learning models (Wang et al., 2016; Wang et al., 2021).

The N leaching and transformation in groundwater, especially denitrification and nitrification, must be considered in other numerical and/or distributed groundwater flow models to accurately predict NO_3^--N dynamics. The NO_3^--N in groundwater tends to be the most sensitive to NO_2^--N, indicating that biotic factors play critical roles in controlling the N transformation (Yang et al., 2012). These biochemical processes cause the difficulty and challenge of building and verifying groundwater flow and solute transport models. It is essential to study microbial communities and growth response to changes in N and C substrates and environmental factors to gain better insights into N transformation processes and rates (Nikolenko et al., 2018). It should be noted that except for the commonly considered nitrification and

denitrification processes identified in this study, other N transformation processes in shallow groundwater are also possible. For instance, NO_2^--N accumulation in denitrification can provide the substrate for anammox (Smith et al., 2015), DNRA (Jahangir et al., 2017), and shortcut nitrification-denitrification (Hu et al., 2018). Therefore, it is necessary to measure the N transformation rates using the ^{15}N tracing method, and analyze microbial communities based on in situ experiments and laboratory simulation of the groundwater environment to precisely understand the fate of N in groundwater in future studies.

5. Conclusions

Nitrate as the primary source of inorganic N pollutants in shallow groundwater, showed highly variable spatiotemporal patterns in an irrigated agricultural area, the NCP. Monthly soil physiochemical data, groundwater quality data, and groundwater NO_3^--N isotopic composition data were measured and analyzed from May 2017 to April 2019 in the study area. This research focused on predicting spatial and intra-annual variations of shallow groundwater NO_3^--N and evaluating their main effect factors and processes. The random forest model, as a simplified approach compared to numerical and distributed hydrological models, performed well in predicting the spatial and intra-annual variations of NO_3^--N in groundwater with R^2 value of 0.93 and 0.92, RMSE value of 4.94 and 3.87, and MAE values of 2.10 and 2.89 for the training and test datasets, respectively. The application of the random forest model may have important implications for groundwater NO_3^--N prediction in other regions worldwide. Evaluation of the importance of the effect factors emphasized the roles of N transformation, including denitrification and nitrification,

in controlling spatiotemporal variations of NO_3^--N in addition to N leaching. The impacts of soil SON on groundwater NO_3^--N was the greatest among different forms of N in surface soil. The temporal increase of NO_3^--N was mainly attributed to NO_3^--N leaching, while the temporal decrease of NO_3^--N can be attributed to denitrification. Although the N leaching usually decreases with the increase of groundwater table depth, nitrification along the groundwater flow path will adversely affect groundwater quality in deep vadose zone areas. Monitoring and management of SON in soil and DON in groundwater will become increasingly important since agronomists and policy makers widely recommend the use of manure instead of chemical fertilizers in developing and developed countries. The groundwater NO_3^--N is significantly related to nitrite which is an indicator of biotic factors, but groundwater NO_3^--N is less sensitive to other environmental factors. The prediction of groundwater NO_3^--N dynamics using hydrological or biochemical models should address all forms of N leaching and transformation in groundwater, which is still a considerable challenge due to the involvement of biological factors. The ability to identify the N transformation process and quantify the N transformation rates is urgently needed and deserves further attention through the adoption of microbiological techniques and ^{15}N tracing methods based on in situ and laboratory groundwater experiments.

Declaration of Competing Interest: The authors declare no conflict of interest.

Data availability: The data analyzed and presented in this study are openly available.

Acknowledgment: This research was funded by the National Natural Science Foundation of China (No. 51609084). The authors sincerely thank the anonymous reviewers for their insightful comments.

References

[1] Amit Y, Geman D. 1997. Shape quantization and recognition with randomized trees. Neural Comput.; 9: 1545-1588. https://doi.org/10.1162/neco.1997.9.7.1545

[2] Awais M, Aslam B, Maqsoom A, Khalil U, Ullah F, Azam S, et al. 2021. Assessing nitrate contamination risks in groundwater: A machine learning approach. Appl. Sci.; 11: 10034. https://doi.org/10.3390/app112110034

[3] Bagherzadeh F, Mehrani M-J, Basirifard M, Roostaei J. 2021. Comparative study on total nitrogen prediction in wastewater treatment plant and effect of various feature selection methods on machine learning algorithms performance. J. Water Process. Eng.; 41: 102033. https://doi.org/10.1016/j.jwpe.2021.102033

[4] Band SS, Janizadeh S, Pal SC, Chowdhuri I, Siabi Z, Norouzi A, et al. 2020. Comparative analysis of artificial intelligence models for accurate estimation of groundwater nitrate concentration. Sensors; 20. https://doi.org/10.3390/s20205763

[5] Bergamasco MAM, Braos LB, Guidini Lopes I, Cruz MCP. 2019. Nitrogen mineralization and nitrification in two soils with different pH levels. Commun. Soil Sci. Plant Anal.; 50: 2873-2880. https://doi.org/10.1080/00103624.2019.1689250

[6] Biddau R, Cidu R, Da Pelo S, Carletti A, Ghiglieri G, Pittalis D. 2019. Source and fate of nitrate in contaminated groundwater systems: Assessing spatial and temporal variations by hydrogeochemistry and multiple stable isotope tools. Sci. Total Environ.; 647: 1121-1136. https://doi.org/10.1016/j.scitotenv.2018.08.007

[7] Bohrerova Z, Stralkova R, Podesvova J, Bohrer G, Pokorny E. 2004. The relationship between redox potential and nitrification under different sequences of crop rotations. Soil Tillage Res.; 77: 25-33. https://doi.org/10.1016/j.still.2003.10.006

[8] Breiman L. 2001. Random Forests. Mach. Learn.; 45: 5–32. https://doi.org/10.1023/A:1010933404324

[9] Castrillo M, García ÁL. 2020. Estimation of high frequency nutrient concentrations from water quality surrogates using machine learning methods. Water Res.; 172: 115490. https://doi.org/10.1016/j.watres.2020.115490

[10] Chlingaryan A, Sukkarieh S, Whelan B. 2018. Machine learning approaches for crop yield prediction and nitrogen status estimation in precision agriculture: A review. Comput. Electron. Agric.; 151: 61-69. https://doi.org/10.1016/j.compag.2018.05.012

[11] Coppola Jr EA, Rana AJ, Poulton MM, Szidarovszky F, Uhl VW. 2005. A neural network model for predicting aquifer water level elevations. GROUNDWATER; 43: 231-241. https://doi.org/10.1111/j.1745-6584.2005.0003.x

[12] Dinçer AR, Kargi F. 1999. Salt inhibition of nitrification and denitrification in saline wastewater. Environ. Technol.; 20: 1147-1153. https://doi.org/10.1080/09593332008616912

[13] Du R, Peng Y, Cao S, Li B, Wang S, Niu M. 2016. Mechanisms and microbial structure of partial denitrification with high nitrite accumulation. Appl. Microbiol. Biotechnol.; 100: 2011-2021. https://doi.org/10.1007/s00253-015-7052-9
[14] El Amri A, M'Nassri S, Nasri N, Nsir H, Majdoub R. 2022. Nitrate concentration analysis and prediction in a shallow aquifer in central-eastern Tunisia using artificial neural network and time series modelling. Environ. Sci. Pollut. Res. Int.; 29: 43300-43318. https://doi.org/10.1007/s11356-021-18174-y
[15] Famiglietti JS, Ferguson G. 2021. The hidden crisis beneath our feet. Science; 372: 344-345. https://doi.org/10.1126/science.abh2867
[16] Foulquier A, Malard F, Mermillod-Blondin F, Montuelle B, Dolédec S, Volat B, et al. 2011. Surface water linkages regulate trophic interactions in a groundwater food web. Ecosystems; 14: 1339-1353. http://doi.org/10.1007/s10021-011-9484-0
[17] Gan L, Huang G, Pei L, Gan Y, Liu C, Yang M, et al. 2022. Distributions, origins, and health-risk assessment of nitrate in groundwater in typical alluvial-pluvial fans, North China Plain. Environ. Sci. Pollut. Res. Int.; 29: 17031-17048. https://doi.org/10.1007/s11356-021-17067-4
[18] Gao Z, Han C, Yuan S, Liu J, Peng Y, Li C. 2022. Assessment of the hydrochemistry, water quality, and human health risk of groundwater in the northwest of Nansi Lake Catchment, north China. Environ. Geochem. Health; 44: 961-977. https://doi.org/10.1007/s10653-021-01011-z
[19] Guo H, Ye C, Zhang H, Pan S, Ji Y, Li Z, et al. 2017. Long-term nitrogen & phosphorus additions reduce soil microbial respiration but increase its temperature sensitivity in a Tibetan alpine meadow. Soil Biol. Biochem.; 113: 26-34. https://doi.org/10.1016/j.soilbio.2017.05.024
[20] Hayatsu M, Kosuge N. 1993. Autotrophic nitrification in acid tea soils. Soil Sci. Plant Nutr.; 39: 209-217. https://doi.org/10.1080/00380768.1993.10416992
[21] He S, Wu J, Wang D, He X. 2022. Predictive modeling of groundwater nitrate pollution and evaluating its main impact factors using random forest. Chemosphere; 290: 133388. https://doi.org/10.1016/j.chemosphere.2021.133388
[22] Hinkle SR, Tesoriero AJ. 2014. Nitrogen speciation and trends, and prediction of denitrification extent, in shallow US groundwater. J. Hydrol.; 509: 343-353. https://doi.org/10.1016/j.jhydrol.2013.11.048
[23] Hood-Nowotny R, Umana NH-N, Inselbacher E, Oswald- Lachouani P, Wanek W. 2010. Alternative methods for measuring inorganic, organic, and total dissolved nitrogen in soil. Soil Sci. Soc. Am. J.; 74: 1018-1027. https://doi.org/10.2136/sssaj2009.0389
[24] Hu W, Zhou Y, Min X, Liu J, Li X, Luo L, et al. 2018. The study of a pilot-scale aerobic/Fenton/anoxic/aerobic process system for the treatment of landfill leachate. Environ. Technol.; 39: 1926-1936. https://doi.org/10.1080/09593330.2017.1344325
[25] Jahangir MMR, Fenton O, Müller C, Harrington R, Johnston P, Richards KG. 2017. In situ denitrification and DNRA rates in groundwater beneath an integrated constructed wetland. Water Res.; 111: 254-264.

https://doi.org/10.1016/j.watres.2017.01.015
[26] Jendia AH, Hamzah S, Abuhabib AA, El-Ashgar NM. 2020. Removal of nitrate from groundwater by eggshell biowaste. Water Supply; 20: 2514-2529. http://doi.org/10.2166/ws.2020.151
[27] Ji W, Xiao J, Toor GS, Li Z. 2021. Nitrate-nitrogen transport in streamwater and groundwater in a loess covered region: Sources, drivers, and spatiotemporal variation. Sci. Total Environ.; 761: 143278. https://doi.org/10.1016/j.scitotenv.2020.143278
[28] Knoll L, Breuer L, Bach M. 2019. Large scale prediction of groundwater nitrate concentrations from spatial data using machine learning. Sci. Total Environ.; 668: 1317-1327.https://doi.org/10.1016/j.scitotenv.2019.03.045
[29] Lasserre F, Razack M, Banton O. 1999. A GIS-linked model for the assessment of nitrate contamination in groundwater. J. Hydrol.; 224: 81-90. https://doi.org/10.1016/S0022-1694(99)00130-4
[30] Li Z, Zhang Q, Qiao Y, Leng P, Zhang Q, Du K, et al. 2021. Influence of the shallow groundwater table on the groundwater N_2O and direct N_2O emissions in summer maize field in the North China Plain. Sci. Total Environ.; 799: 149495. https://doi.org/10.1016/j.scitotenv.2021.149495
[31] Liu J, Liu Q, Yang H. 2016. Assessing water scarcity by simultaneously considering environmental flow requirements, water quantity, and water quality. Ecol. Indic.; 60: 434-441. https://doi.org/10.1016/j.ecolind.2015.07.019
[32] Liu Y, Xin J, Wang Y, Yang Z, Liu S, Zheng X. 2022. Dual roles of dissolved organic nitrogen in groundwater nitrogen cycling: Nitrate precursor and denitrification promoter. Sci. Total Environ.; 811: 151375. https://doi.org/10.1016/j.scitotenv.2021.151375
[33] Nikolenko O, Jurado A, Borges AV, Knöller K, Brouyère S. 2018. Isotopic composition of nitrogen species in groundwater under agricultural areas: A review. Sci. Total Environ.; 621: 1415-1432. https://doi.org/10.1016/j.scitotenv.2017.10.086
[34] Osaka Ki, Ohte N, Koba K, Yoshimizu C, Katsuyama M, Tani M, et al. 2010. Hydrological influences on spatiotemporal variations of $\delta^{15}N$ and $\delta^{18}O$ of nitrate in a forested headwater catchment in central Japan: Denitrification plays a critical role in groundwater. Journal of Geophysical Research: Biogeosciences; 115. https://doi.org/10.1029/2009JG000977
[35] Ouedraogo I, Defourny P, Vanclooster M. 2019. Validating a continental-scale groundwater diffuse pollution model using regional datasets. Environ. Sci. Pollut. Res. Int.; 26: 2105-2119. https://doi.org/10.1007/s11356-017-0899-9
[36] Pang Y, Wang J. 2021. Various electron donors for biological nitrate removal: A review. Sci. Total Environ.; 794: 148699. https://doi.org/10.1016/j.scitotenv.2021.148699
[37] Peng B, Liang H, Wang S, Gao D. 2020. Effects of DO on N_2O emission during biological nitrogen removal using aerobic granular sludge via shortcut simultaneous nitrification and denitrification. Environ. Technol.; 41: 251-259.

https://doi.org/10.1080/09593330.2018.1494757
[38] Pennino MJ, Leibowitz SG, Compton JE, Hill RA, Sabo RD. 2020. Patterns and predictions of drinking water nitrate violations across the conterminous United States. Sci. Total Environ.; 722: 137661. https://doi.org/10.1016/j.scitotenv.2020.137661
[39] Razzaghi F, Plauborg F, Jacobsen S-E, Jensen CR, Andersen MN. 2012. Effect of nitrogen and water availability of three soil types on yield, radiation use efficiency and evapotranspiration in field-grown quinoa. Agric. Water Manag.; 109: 20-29. https://doi.org/10.1016/j.agwat.2012.02.002
[40] Rivas A, Singh R, Horne D, Roygard J, Matthews A, Hedley MJ. 2017. Denitrification potential in the subsurface environment in the Manawatu River catchment, New Zealand: Indications from oxidation-reduction conditions, hydrogeological factors, and implications for nutrient management. J. Environ. Manag.; 197: 476-489. https://doi.org/10.1016/j.jenvman.2017.04.015
[41] Rivett MO, Buss SR, Morgan P, Smith JWN, Bemment CD. 2008. Nitrate attenuation in groundwater: A review of biogeochemical controlling processes. Water Res.; 42: 4215-4232. https://doi.org/10.1016/j.watres.2008.07.020
[42] Sexstone AJ, Parkin TB, Tiedje JM. 1985. Temporal response of soil denitrification rates to rainfall and irrigation. Soil Sci. Soc. Am. J.; 49: 99-103. https://doi.org/10.2136/sssaj1985.03615995004900010020x
[43] Shen Z, Xin J, Wu H, Jiang Z, Peng H, Xu F, et al. 2023. Kinetic and molecular evidence for DON transformation in the deep vadose zone: Important implications for soil nitrogen budgeting and groundwater nitrate management. J. Hydrol.; 616: 128782. https://doi.org/10.1016/j.jhydrol.2022.128782
[44] Singh BK, Bardgett RD, Smith P, Reay DS. 2010. Microorganisms and climate change: terrestrial feedbacks and mitigation options. Nat. Rev. Microbiol.; 8: 779-790. http://doi.org/10.1038/nrmicro2439
[45] Smarra F, Jain A, de Rubeis T, Ambrosini D, D'Innocenzo A, Mangharam R. 2018. Data-driven model predictive control using random forests for building energy optimization and climate control. Appl. Energy; 226: 1252-1272. https://doi.org/10.1016/j.apenergy.2018.02.126
[46] Smith RL, Böhlke JK, Song B, Tobias CR. 2015. Role of anaerobic ammonium oxidation (anammox) in nitrogen removal from a freshwater aquifer. Environ. Sci. Technol.; 49: 12169-12177. https://doi.org/10.1021/acs.est.5b02488
[47] Spoelstra J, Schiff S, Elgood R, Semkin R, Jeffries D. 2001. Tracing the sources of exported nitrate in the Turkey Lakes Watershed using $^{15}N/^{14}N$ and $^{18}O/^{16}O$ isotopic ratios. Ecosystems; 4: 536-544. https://doi.org/10.1007/s10021-001-0027-y
[48] Strous M, Kuenen JG, Jetten MS. 1999. Key physiology of anaerobic ammonium oxidation. Appl. Environ. Microbiol.; 65: 3248-50. https://doi.org/10.1128/aem.65.7.3248-3250.1999
[49] Thayalakumaran T, Bristow KL, Charlesworth PB, Fass T. 2008. Geochemical conditions in groundwater systems: Implications for the attenuation of

agricultural nitrate. Agric. Water Manag.; 95: 103-115. https://doi.org/10.1016/j.agwat.2007.09.003

[50] van Es HM, Schindelbeck RR, Jokela WE. 2004. Effect of manure application timing, crop, and soil type on phosphorus leaching. J. Environ. Qual.; 33: 1070-1080. https://doi.org/10.2134/jeq2004.1070a

[51] Vandenbruwane J, De Neve S, Qualls R G, Sleutel S, Hofman G. 2007. Comparison of different isotherm models for dissolved organic carbon (DOC) and nitrogen (DON) sorption to mineral soil. Geoderma, 139(1-2), 144-153. https://doi.org/10.1016/j.geoderma.2007.01.012

[52] Vidon P, Hill AR. 2004. Denitrification and patterns of electron donors and acceptors in eight riparian zones with contrasting hydrogeology. Biogeochemistry; 71: 259-283. http://doi.org/10.1007/s10533-004-9684-1

[53] Vystavna Y, Diadin D, Valeriy Y, Hejzlar J, Vadillo I, Huneau F, et al. 2017. Nitrate contamination in a shallow urban aquifer in East Ukraine: Evidence from hydrochemical, stable nitrate isotope, and land use analysis. Environ. Earth Sci.; 76. https://doi.org/10.1007/s12665-017-6796-1

[54] Wang C, Jiang R, Boithias L, Sauvage S, Sánchez-Pérez JM, Mao X, Han Y, Hayakawa A, Kuramochi K, Hatano R. 2016. Assessing potassium environmental losses from a dairy farming watershed with the modified SWAT model. Agr. Water Manage.; 175, 91-104. https://doi.org/10.1016/j.agwat.2016.02.007

[55] Wang C, Wu D, Mao X, Hou J, Wang L, Han Y. 2021. Estimating soil ammonium adsorption using pedotransfer functions in an irrigation district of the North China Plain. Pedosphere; 31: 157-171. https://doi.org/10.1016/S1002-0160(20)60054-6

[56] Wang Y, Peng J, Cao X, Xu Y, Yu H, Duan G, et al. 2020. Isotopic and chemical evidence for nitrate sources and transformation processes in a plateau lake basin in Southwest China. Sci. Total Environ.; 711: 134856. https://doi.org/10.1016/j.scitotenv.2019.134856

[57] Weitzman JN, Brooks JR, Compton JE, Faulkner BR, Mayer PM, Peachey RE, et al. 2022. Deep soil nitrogen storage slows nitrate leaching through the vadose zone. Agr Ecosyst Environ; 332: 107949. https://doi.org/10.1016/j.agee.2022.107949

[58] Wells NS, Baisden WT, Horton T, Clough TJ. 2016. Spatial and temporal variations in nitrogen export from a New Zealand pastoral catchment revealed by stream water nitrate isotopic composition. Water Resour. Res.; 52: 2840-2854. https://doi.org/10.1002/2015WR017642

[59] Xinxiang City Water Resources Bureau (XCWRB), 2017. Xinxiang City Water Resources Bulletin. http://slj.xinxiang.gov.cn/ggl/1983.html

[60] Xue D, Botte J, De Baets B, Accoe F, Nestler A, Taylor P, et al. 2009. Present limitations and future prospects of stable isotope methods for nitrate source identification in surface- and groundwater. Water Res.; 43: 1159-1170. https://doi.org/10.1016/j.watres.2008.12.048

[61] Yang X, Wang S, Zhou L. 2012. Effect of carbon source, C/N ratio, nitrate and dissolved oxygen concentration on nitrite and ammonium production from denitrification process by Pseudomonas stutzeri D6. Bioresour. Technol.; 104: 65-72. https://doi.org/10.1016/j.biortech.2011.10.026

[62] Zhang Y, Xu B, Guo Z, Han J, Li H, Jin L, et al. 2019. Human health risk assessment of groundwater arsenic contamination in Jinghui irrigation district, China. J. Environ. Manag.; 237: 163-169. https://doi.org/10.1016/j.jenvman.2019.02.067

[63] Zhao B, Zhang J, Yu Y, Karlen DL, Hao X. 2016. Crop residue management and fertilization effects on soil organic matter and associated biological properties. Environ. Sci. Pollut. Res.; 23: 17581-17591. http://doi.org/10.1007/s11356-016-6927-3

[64] Zhou J, Green M, Shaviv A. 2003. Mineralization of organic N originating in treated effluent used for irrigation. Nutr. Cycl. Agroecosyst.; 67: 205-213. https://doi.org/10.1023/B:FRES.0000003599.60911.a2